TITLE: Fluorescence hybridization chain reaction enables localization of multiple molecular classes combined with plant cell ultrastructure

AUTHORS: Yunqing Yu[1,3], David Huss[1,2], Mao Li[3], Janithri S. Wickramanayake[2], Sébastien Bélanger[3], Anastasiya Klebanovych[2], Blake Meyers[3,4], Elizabeth A. Kellogg[3], Kirk J. Czymmek[2,*]

[1]Co-first authors

[2]Advanced Bioimaging Laboratory, Donald Danforth Plant Science Center, 975 N Warson Rd, Saint Louis, MO 63132, USA

[3]Donald Danforth Plant Science Center, 975 N Warson Rd, Saint Louis, MO 63132, USA

[4]Division of Plant Science & Technology, University of Missouri - Columbia, Columbia, MO 65211, USA

*Corresponding Author: Kirk J Czymmek (kczymmek@danforthcenter.org)

ABSTRACT (max 350 words)

Background. Recent developments in hybridization chain reaction (HCR) have enabled robust simultaneous localization of multiple mRNA transcripts using fluorescence *in situ* hybridization (FISH). Once multiple split initiator oligonucleotide probes bind their target mRNA, HCR uses DNA base-pairing of fluorophore-labeled hairpin sets to self-assemble into large polymers, amplifying the fluorescence signal and reducing non-specific background. Few studies have applied HCR in plants, despite its demonstrated utility in whole mount animal tissues and cell culture. Our aim was to optimize this technique for sectioned plant tissues embedded with paraffin and methacrylate resins, and to test its utility in combination with immunolocalization and subsequent correlation with cell ultrastructure using scanning electron microscopy.

Results. Application of HCR to 10 µm paraffin sections of 17-day-old *Setaria viridis* (green millet) inflorescences using confocal microscopy revealed that the transcripts of the transcription factor *KNOTTED 1* (*KN1*) were localized to developing floret meristem and vascular tissue while *SHATTERING 1* (*SH1*) and *MYB26* transcripts were co-localized to the breakpoint below the floral structures (the abscission zone). We also used methacrylate de-embedment with 1.5 µm and 0.5 µm sections of 3-day-old *Arabidopsis thaliana* seedlings to show tissue specific *CHLOROPHYLL BINDING FACTOR a/b* (*CAB1*) mRNA highly expressed in photosynthetic tissues and *ELONGATION FACTOR 1 ALPHA* (*EF1α*) highly expressed in meristematic tissues of the shoot apex. The housekeeping gene *ACTIN7* (*ACT7*) mRNA was more uniformly distributed with reduced signals using lattice structured-illumination microscopy. HCR using 1.5 µm methacrylate sections was followed by backscattered imaging and scanning electron microscopy thus demonstrating the feasibility of correlating fluorescent localization with ultrastructure.

Conclusion. HCR was successfully adapted for use with both paraffin and methacrylate de-embedment on diverse plant tissues in two model organisms, allowing for concurrent cellular and subcellular localization of multiple mRNAs, antibodies and other affinity probe classes. The mild hybridization conditions used in HCR made it highly amenable to observe immunofluorescence in the same section. De-embedded semi-thin methacrylate sections with HCR were compatible with correlative electron microscopy approaches. Our protocol provides numerous practical tips for successful HCR and affinity probe labeling in electron microscopy-compatible, sectioned plant material.

KEY WORDS: hybridization chain reaction (HCR), fluorescent *in situ* hybridization (FISH), multiplex, Formalin fixed Paraffin Embedded (FFPE), methacrylate de-embedment, plant, immunofluorescence, scanning electron microscopy (SEM), correlative microscopy, correlative light and electron microscopy (CLEM)

BACKGROUND

Characterization of RNA molecules and their downstream products at the cellular and subcellular level is essential to understand gene function and transcript regulation within the complex cellular environment of multicellular organisms including plants. Spatiotemporal expression patterns of genes can be detected using promoter-driven reporter genes expressed in transgenic plants, or *in situ* hybridization (ISH). The latter is particularly useful in species where generation of transgenic plants is unavailable, time-consuming or costly. Traditional ISH uses long (150-1500 bases) anti-sense, single-stranded RNA riboprobes tagged with a hapten such as digoxygenin (DIG), biotin, or fluorescein with uracil (1–3).The haptens are subsequently detected by specific antibodies conjugated with alkaline phosphatase, which catalyzes colorimetric reactions on chromogenic substrates such as nitroblue tetrazolium/ 5-bromo- 4-chloro-3-indolyl-phosphate (NBT/BCIP). While this technique has been successfully applied in

68 both whole mount and sectioned tissues in plants (4–9), the diffusion of chromogenic deposition
69 may obscure cellular and subcellular details of signal, and the use of proteases to increase
70 probe permeability may be detrimental to tissue morphology. Additionally, colorimetric ISH does
71 not allow simultaneous detection of multiple genes or other molecules, and therefore is not
72 suitable for studying gene co-expression or the spatial distribution of RNA and other molecules
73 such as proteins and polysaccharides.

74 Fluorescent ISH (FISH) is an alternative technique that is compatible with multiplexed target
75 detection. FISH relies on fluorophores directly or indirectly conjugated with RNA or DNA probes
76 to visualize signals. Fluorophores can be conjugated to primary antibodies that target RNA
77 probes labeled with a hapten or secondary antibodies and visualized under a fluorescence
78 microscope. However, since this approach lacks an amplification component as in colorimetric
79 ISH, it may not provide sufficient signal-to-noise for visualizing weakly expressed genes.
80 Various techniques have been developed to enhance signal, either through increasing probe
81 numbers, improving detection sensitivity or amplifying the original signal. Single molecule FISH
82 (smFISH) uses a large set of fluorophore-labeled, short, DNA oligonucleotide probes (20 – 22
83 nucleotides (nt)) dispersed along the target mRNA (10). Super-resolution microscopy can
84 further enhance the detection sensitivity and localization precision of smFISH (11). Direct
85 labeling of DNA probes preserves spatial resolution of the target mRNA compared to methods
86 using enzymes to catalyze chromogenic or fluorogenic reactions. However, direct conjugation of
87 fluorophores to individual probes can be expensive when multiple genes are targeted.

88 To improve sensitivity, signal amplification technologies have been developed including
89 tyramide signal amplification (TSA) (12), rolling circle amplification (RCA) (9,13), RNAscope (14)
90 and hybridization chain reaction (HCR) (15,16). TSA uses primary antibody conjugated
91 horseradish peroxidase to activate the binding of fluorophore-labeled tyramide with tyrosine
92 residues at or near the peroxidase reaction site (17). TSA has been used to differentiate nuclear

93 and cytoplasmic RNA in Formalin-Fixed, Paraffin Embedded (FFPE) *Arabidopsis* shoot apices
94 (12). Rolling circle amplification (RCA) together with padlock probes and barcoding system
95 allows highly multiplexed *in situ* sequencing by hybridization and has been applied in FFPE
96 maize shoot apex and *Arabidopsis* whole mount root tips to target 90 and 28 genes,
97 respectively (9,13,18,19). The RNAscope® system from ACD Bio (Newark, CA) uses a set of
98 probe pairs, each linked with one half of a Pre-Amp sequence to limit non-specific signal,
99 followed by amplifying the specific fluorescent signal by building a branched DNA molecule (14).
100 RNAscope has been adapted to plant tissues, including FFPE maize and cassava leaf (20,21)
101 and cryo-sectioned barley leaf (22).

102 Alternatively, HCR FISH adopts an enzyme-free approach and uses two kinetically trapped DNA
103 hairpins linked with a fluorophore. Version 3 enhancements of HCR FISH (23) uses a set of
104 paired 25 nt probes separated by 2 nt, each linked with half of an initiator sequence, resulting in
105 a 45 nt length for each probe. Only when both probes in a pair are fully hybridized to the target,
106 does the full-length initiator sequence become available. This initiates the hybridization and
107 opening of hairpin 1 (H1), which in turn hybridizes and opens hairpin 2 (H2). H2 then unfolds,
108 revealing a complementary strand to H1, and the process is repeated to eventually assemble
109 into a double-stranded polymer of alternated overlapping H1 and H2. Since H1 and H2 are each
110 conjugated to a fluorophore, the result is a large fluorescent polymer tethered to the site of each
111 initial probe pair binding event (Fig. 1). Five unique initiator sequences allow for simultaneous
112 hybridization and detection of multiple target mRNAs (23). HCR FISH has the benefit of being
113 sensitive and quantitative (24). The reagents can be prepared in house or are commercially
114 available through Molecular Instruments (Los Angeles, CA). Recently, HCR FISH has been
115 applied in wholemount tissues of *Arabidopsis* inflorescences and *Arabidopsis*, maize and
116 sorghum roots (13,25,26).

117 Thus far, all the above techniques use wholemount or FFPE processed plant tissues. Although
118 subcellular localization has been demonstrated, due to the inherent nature of the typical FFPE
119 fixation and wax-based embedment strategy, in most instances ultrastructural quality is severely
120 compromised or simply not practical. *In situ* hybridization at the transmission electron
121 microscopy level has also been successfully applied in plant sections for abundant mRNA
122 targets and has the benefit of providing sub-cellular ultrastructural context to its distribution (27–
123 29). However, these approaches were limited to a single mRNA target population and
124 combination with immunolocalization proteins was not employed. Methacrylate resins for protein
125 and/or nucleic acids have been successfully applied with improved morphology and subcellular
126 localization compared to FFPE (5,30,31). Furthermore, in this approach, the semi-thin
127 methacrylate sections which are de-embedded with acetone, improved probe accessibility and
128 thus labeling density for light microscopy. Aldehyde fixation and resin de-embedment would be
129 expected to negatively impact morphology compared to osmium tetroxide fixed versus non-de-
130 embedment acrylic and/or epoxy resins. However, this strategy is a recognized compromise to
131 balance adequate probe signal and provide reasonable cellular structure and nevertheless, far
132 superior to paraffin.

133 Here, we demonstrate the utility of HCR FISH in sectioned FFPE and methyl methacrylate
134 embedded samples. Using an optimized protocol, we show multiplex HCR FISH with the
135 capacity of combining immunofluorescence and other affinity probes with seedlings of
136 *Arabidopsis thaliana* and inflorescence of *Setaria viridis*. Furthermore, for the first time, we
137 correlated HCR FISH with electron microscopy images from the same section, enabling the
138 potential for high spatial resolution of the subcellular localization of mRNA, proteins, and other
139 cell molecules with the long-term goal to localize cellular pathways.

140 **RESULTS**

141 **HCR detected low-level gene expression in FFPE samples**

142 In order to establish and optimize an HCR FISH protocol for FFPE plant material, we first used
143 panicles from 17-day-old *Setaria viridis*, in which colorimetric ISH was previously demonstrated
144 (12,32). Three transcription factors, *SHATTERING1* (*SH1*, Sevir.9G153200.1), *MYB26*
145 (Sevir.5G293800.1) and *KNOTTED-1* (*KN1*, Sevir.9G107600.1) were used for multiplexed HCR
146 FISH. Both *SH1* and *MYB26* were specifically enriched in the abscission zone below the
147 spikelet based on our previous RNA-Seq analysis (32). However, while *SH1* can be validated by
148 colorimetric ISH, *MYB26* failed to be detected by this method, possibly due to its low absolute
149 expression level (Fig. S1) (32) *KN1* is highly expressed in the apical meristem except the
150 epidermal layer, and the vascular tissues (Fig. S1) (33,34). For each gene, seven to eight pairs
151 of probes spanning the coding sequence (CDS) and 3' untranslated region (UTR) were
152 designed, and each probe carried half of a unique initiator, specifically, Initiator B2 for *SH1*, B3
153 for *MYB26* and B4 for *KN1* (Table S1). The initiators can be recognized by specific hairpins
154 conjugated to spectrally separated fluorophores (Alexa Fluor 546 for B2, Alexa Fluor 647 for B3,
155 and Alexa Fluor 488 for B4), allowing simultaneous amplification and detection for all three
156 genes. We observed above background signals of *SH1* and *MYB26* in the abscission zone (AZ),
157 and *KN1* in the floral meristem (Fig. 2A), consistent with the literature (32,33). Negative controls
158 for HCR experiments included samples without probes or hairpins to assess autofluorescence
159 of the tissue (Fig. 2B), and samples with hairpins alone to indicate non-specific amplification
160 (NSA) (Fig. 2C). These controls were essential in determining true signals from background in
161 plant materials, as autofluorescence was observed in our samples most notably with green (488
162 AF) and red (546 AF) emission channels (Fig. 2B). Our initial experiments using probes without
163 purification identified substantial NSA, especially for the MYB26 probes. Polyacrylamide gel
164 electrophoresis (PAGE) purification of the probes prior to HCR, selecting probe sizes of 45 nt,
165 greatly reduced NSA (Fig. 2C). We therefore used purified probes for subsequent experiments.

166 **HCR simultaneously detected mRNA of multiple genes**

167 Next, we tested the capacity of HCR in semi-thin, methyl methacrylate, de-embedded samples.
168 We used 3-day-old *Arabidopsis thaliana* seedlings, in which methacrylate embedded samples
169 were previously demonstrated for colorimetric ISH (5). HCR probe sets were designed against
170 *CHLOROPHYLL BINDING FACTOR a/b* (*CAB1*, At1G29930) expressed in photosynthetic
171 tissues, *ELONGATION FACTOR 1 ALPHA* (*EF1*α, At1G07940) expressed in actively dividing
172 cells, and *ACTIN 7* (*ACT7*, At5G09810) expressed ubiquitously (Table S1). *CAB1*, *EF1*α and
173 *ACT7* were probed using B2-Alexa546, B3-Alexa647 and B4-Alexa488, respectively. The
174 formation of hairpin polymers in the presence of a probe pair was confirmed *in vitro* (Fig. S2).
175 HCR applied to 10 μm FFPE sections using confocal microscopy detected signals in the
176 chloroplast-containing cells of cotyledons, shoot apex and hypocotyls for CAB1 and shoot apex
177 for EF1α (Fig. 3A and Fig. S3, A and C). However, the *ACT7* signal could not be readily
178 differentiated from the background (data not shown) using our confocal microscope. Semi-thin
179 methacrylate samples (1.5 μm) yielded similar results (Fig. S3, B and D), even for sections at
180 thin as 0.5 μm (Fig. S4), but the morphological properties of the tissues were far superior to the
181 paraffin sections (Fig. 2A, compare Fig. S3 C and D to Fig. S3 A and C). In addition, reduced
182 background signals were observed from these tissues and probes (Fig. 2, B and C).

183 **Super-resolution microscopy improved detection sensitivity and resolution of HCR**
184 **signals**

185 We were unable to detect ACT7 HCR signal in either paraffin or methacrylate embedded
186 sections using our confocal system (Fig 4A). To determine if this was simply due to low-intensity
187 signals, we applied a super-resolution approach with high-sensitivity, complementary metal-
188 oxide-semiconductor (CMOS) cameras and lattice structured illumination microscopy (SIM). In
189 both 10 μm paraffin and 1.5 μm methacrylate embedded sections, we observed individual

190 puncta of Alexa Fluor 488 signal in samples incubated with *ACT7* probes (Fig. 4, B and D) but
191 not with the hairpin control (Fig. 4, C and E), suggesting that the observed signal was not due to
192 autofluorescence or NSA. This also demonstrated the utility of SIM-based super-resolution
193 microscopy in detecting low-intensity HCR signals in plant sections.

194 **HCR FISH can be combined with immunofluorescence in both FFPE and methacrylate**
195 **sections**

196 To test the compatibility of HCR with immunolabeling, we performed a standard
197 immunolocalization protocol after the completion of HCR prior to imaging. With FFPE *Setaria*
198 inflorescences, we observed elevated *SH1* transcript signals restricted in the AZ and the
199 ubiquitous cytoskeletal actin proteins (Fig. 5A), while very low background signals were
200 observed in negative controls with the corresponding hairpins for B2-Alexa546 system and anti-
201 rabbit DyLight650 secondary antibody (Fig. 5B). Likewise, using *Arabidopsis* seedlings
202 embedded in methacrylate, *CAB1* transcripts were readily detected in cotyledons and at low
203 levels in the shoot apex as expected. In the same section, unesterified homogalacturonan, a
204 type of pectic polymer, was detected uniformly in the cell wall using antibody LM19 (Fig. 5C).
205 NSA and non-specific secondary antibody negative controls in sections from the same biological
206 samples demonstrated specificity of our labeled probes (Fig. 5D).

207 **Linear spectral unmixing improved probe signal separation from plant autofluorescence**

208 In some instances, plant cell autofluorescence, which could vary based on tissue and cell type,
209 interfered with our ability to cleanly delineate signal from background, especially when low-
210 intensity signals/expression were observed. To address this, we evaluated the use of spectral
211 confocal microscopy using linear unmixing of reference signals versus the traditional bandpass
212 filter equivalent (559-694 nm) of fluorescence HCR from Alexa Fluor 647 *EF1α* (compare Figs
213 S5 A and B). It can be readily observed that while some puncta were reliably delineated from

214 cytoplasmic background autofluorescence in the bandpass equivalent (Fig. S5 B blue arrow) a
215 number of puncta overlapped with elevated autofluorescence in chloroplasts, for example (Fig.
216 S5 B white arrows), making definitive localization problematic. The corresponding arrows in the
217 spectrally unmixed data (Fig. S5 A) were readily separated and delineated from
218 autofluorescence background. Furthermore, to better understand the actual spectra in relation
219 to plant autofluorescence with our selected fluorophores and the excitation and emission
220 characteristics of our spectral confocal (ZEISS LSM980 with Quasar detector), we created
221 reference spectra of the pure fluorophores (Calcofluor White and Alexa Fluor 647) from Fig. S5
222 A & B and autofluorescence used in our test system under identical image acquisition conditions
223 (Figs. S5 C & D). The raw (Fig. S5 C) and normalized (Fig. S5 D) spectra showed the dominant
224 broad spectrum autofluorescence covering a large swath of green and red wavelengths, while
225 tailing off rapidly at shorter blue wavelength and longer red wavelengths. These data
226 emphasized the value of using longer red wavelength fluorophores along with standard
227 bandpass strategies, particularly when low-intensity signals might be anticipated, or in general
228 for best signal-to-noise. We assessed this spectral linear unmixing strategy in methacrylate
229 sections over a large spectral range (411-694 nm) and were able to obtain excellent and clean
230 signal separation with an *A. thaliana* meristem labeled with Calcofluor White (Fig. 6 A), plant
231 autofluorescence (Fig. 6 B), HCR *EF1α* (Fig. 6 C) and HCR CAB1 (Fig. 6 D) and all probes
232 combined without (Fig. 6 E) and with autofluorescence in the merged images.

233 **Correlative microscopy allowed visualization of cell ultrastructure with HCR FISH**

234 One of our goals was to assess the feasibility of HCR localization (and potentially other probes)
235 with ultrastructure. Since methacrylate de-embedded samples at 1.5 µm significantly improved
236 cellular morphology of the tissues compare to FFPE and allowed for robust localization using
237 fluorescence, we further tested whether the section quality was suitable for ultrastructural
238 observations using backscatter electron detections with field emission scanning electron

239 microscopy (FESEM). In our initial efforts, we found that 1.5 μm sections of the 3-day-old *A.*
240 *thaliana* meristem at 50 nm x-y pixel resolution allowed the visualization of the cell wall,
241 vacuoles, nucleus, mitochondria, and cytoplasm (Fig. S6 A). Using 50 nm x-y pixel resolution
242 with FESEM was convenient and efficient to perform large area mapping in a reasonable period
243 to assess overall morphology and tissue quality. However, as expected, 5 nm x-y pixel
244 resolution notably improved the clarity of the same sample/location structures (compare Fig. S6
245 A with B) and more definitive cell details. Nevertheless, with backscatter FESEM, 1.5 μm was
246 too thick and loss of clarity prevented delineation of small organelles or sub-organelle features.
247 We therefore sought to identify a balanced thickness producing sufficient fluorescence signals
248 using fluorescence microscopy and ultrastructural detail. While screening a number of plant
249 tissue types and thicknesses (e.g., Fig. S6), we determined that 0.5 μm methacrylate de-
250 embedded sections provided improvements in clarity as shown in these *A. thaliana* root tip cells
251 at 5 nm pixel resolution (Fig. S6 C and D). Specifically, in the root tissue, the nuclear envelope,
252 endoplasmic reticulum, mitochondria, and cristae were readily identified and resolved. Using the
253 previously established probe set, we successfully detected HCR FISH signals for *EF1α* in 0.5
254 μm methacrylate sections of 3-day-old seedling *A. thaliana* cotyledon (Fig. S4). Importantly,
255 following fluorescence imaging, the same sections went through additional osmium tetroxide
256 fixation and heavy metal staining steps to enhance and reveal subcellular structure with FESEM
257 with recognizable nuclei, vacuoles and chloroplasts (Fig. 7). Overlay of the ultrastructure images
258 with HCR FISH found that most of the mRNAs are localized in the cytoplasm, although sporadic
259 HCR puncta were observed in individual nuclei and the cell wall (Fig. 7).

260 **DISCUSSION**

261 **Optimization of an HCR FISH protocol for plant sections**

262 HCR FISH was initially developed for whole-mount animal tissues (15,23) and more recently
263 also applied in whole-mount plant materials (25). Our study is the first to apply HCR FISH in

264 plant sections, being suitable for a wide range of tissue types regardless of thickness and
265 composition and opens the possibility to be combined with correlative ultrastructural studies.
266 Here we provide protocols for both FFPE and methacrylate embedded tissues, as they have
267 unique applications with inherent benefits and limitations. FFPE samples are routinely available
268 and it's straightforward to section large tissue areas and produce much thicker sections that
269 generally contain a higher number of target mRNA molecules. However, FFPE samples
270 generally provided poor sub-cellular morphological preservation and often had elevated levels of
271 tissue autofluorescence. By contrast, methacrylate embedded, acetone de-embedded tissues
272 demonstrated greatly improved morphological preservation but the reduced number of target
273 molecules in semi-thin sections may limit their use to highly to moderately expressed genes
274 without high quantum efficiency detectors. Additionally, sample sizes with methacrylate sections
275 are relatively small (limited to a few millimeters) restricting the area of tissue that can be
276 examined.

277 Cell wall digestion is required for probe penetration of whole-mount tissues, and proteinase K
278 treatment is an essential step for revealing RNA targets in conventional ISH, which uses
279 hapten-labeled long RNA probes (4,25,35). The split initiator HCR probes are un-modified 45 nt
280 oligonucleotides and therefore can penetrate tissues more easily. Our experiments comparing
281 treatments with and without proteinase K in both FFPE and methacrylate samples did not find a
282 detectable difference in revealing HCR signal; thus, our protocol removed this step and the
283 subsequent paraformaldehyde re-fixation required for conventional ISH, shortening the
284 experimental time. More importantly, avoiding proteinase K treatment better preserved cellular
285 morphology, allowing high-resolution detection of HCR signals at the cellular and subcellular
286 levels and correlative study with FESEM.

287 **Autofluorescence and NSA in HCR FISH**

288 Every HCR experiment should be run with tissue-only and hairpin-only negative controls to
289 discern true signal from background autofluorescence and NSA as plants have numerous
290 autofluorescent components. There are substantial differences in cell wall composition in
291 grasses vs. dicots (grasses a lot more ferulates and coumarates than dicots), which affects
292 fluorescence of the cell wall at some wavelengths. Furthermore, the plant cell wall contains
293 molecules such as lignin, suberin and cutin, that are excited by UV or blue light, and emit violet
294 to green light (36). We specifically avoided using the blue wavelengths for HCR and instead
295 used it for detecting more intense cellulose staining using Calcofluor White or other UV stains,
296 like DAPI for nuclei. Furthermore, Calcofluor White served as a useful alignment tool for
297 correlative FESEM and potentially for multiplex studies. Ultimately, our protocol allowed for
298 successful localization in our phylogenetically diverse test specimen.

299 Another abundant fluorescent molecule in plant tissues is chlorophyll, which is broadly excited,
300 ranging from UV to red light, and emits red and far-red light (36). However, chlorophyll
301 autofluorescence itself did not notably interfere with our experiments, probably due to
302 chlorophyll removal by ethanol and acetone treatment during sample preparation and the fact
303 that our probes were generally cytoplasmic. Generally, glutaraldehyde was avoided in the
304 fixative as it enhances autofluorescence of proteins (36) and limits mRNA accessibility;
305 however, very low levels of glutaraldehyde may be suitable for some labeling experiments, or
306 where enhanced ultrastructural morphology is required (37).

307 Linear unmixing is a common method to remove background autofluorescence (38,39) and
308 would certainly benefit plant studies. While we had limited access for use of linear unmixing in
309 this study, we were able to create reference spectra of all tested fluorophores as well as
310 characterize the spectral properties in *A. thaliana* seedling shoot meristems for linear unmixing.
311 Our analysis showed strong green autofluorescence which decreased at lower energy
312 wavelengths into the red and far-red spectrum. This knowledge is very useful when planning

313 labeling experiments and matching anticipated signal levels from various probes relative to the
314 autofluorescence background. Additionally, and consistent with this observation, punctate
315 autofluorescence was observed in stem structures of the *Setaria* inflorescence at higher levels
316 in Alexa Fluor 488 channel, moderate levels in the Alexa Fluor 546 channel but not detected in
317 Alexa Fluor 647 channel (Fig. 2, Supp Fig. S1). Therefore, serving as a cautionary note,
318 adequate controls described herein were mandatory to verify if non-specific puncta were an
319 issue and if use of Alexa Fluor 647 was more appropriate.

320 Although the HCR probes are all 45 nt in length, probes produced by manufacturers are often
321 non-pure and their lengths vary somewhat. If NSA controls show widespread signal in initial
322 HCR experiments, the probes should be PAGE purified to obtain only full-length
323 oligonucleotides around 45 nt. In our experience, using a glycerol-based antifade mounting
324 medium, labeled sections should be imaged as soon as possible after completing the protocol
325 but will usually maintain signal for about 2 – 3 weeks when stored at 4°C in the dark.

326 **Low intensity HCR FISH signal of ACT7**

327 *ACTIN* genes are often used as housekeeping reference genes to normalize sample differences
328 in differential gene expression quantification, for instance, by quantitative reverse transcription
329 (1). ACT7 is highly expressed in rapidly expanding vegetative tissues, detected by promoter-
330 GUS assays (40). Our inability to definitively detect ACT7 HCR signal with confocal microscopy
331 may have been due to some probe pairs in the set failed to bind their target mRNA properly.
332 Split-initiator probe design of HCR reduces non-specific binding to off-targets (23), but
333 optimization of probes may be still required as in most ISH methods. Alternatively, transcripts in
334 ACT7 may be more uniformly distributed in the plant cytoplasm, as opposed to local high-
335 density clusters where intense foci were more conspicuously observed with *EF1α*.
336 Nevertheless, we did observe ACT7 HCR FISH signal above background controls using SIM
337 super-resolution microscopy. This also demonstrated the value of high-sensitivity cameras and

338 super-resolution microscopy for the detection of low expression levels and resulting
339 fluorescence signals.

340 **Toward quantification in plant sections.**

341 While our efforts focused on developing the localization workflows that allowed for multiple
342 probe classes to be combined with electron microscopy in plant tissues, a natural extension
343 would be the potential for signal quantification. However, in our work, plant sections posed
344 unique challenges in reliable quantification. First, consistency in section thickness must be
345 considered and ensured to be uniform across samples. A housekeeping reference protein, gene
346 or cell wall stain could be used for normalizing this variation but would need to be validated for
347 the target tissues. Second, plant cells are highly variable in cell area and relative cytoplasm,
348 often containing large central vacuoles (that take up ~90% of the entire cell volume) and nearby
349 air spaces that may bias the gross signal quantification per unit area. Thus, if quantification is
350 intended, measurements should account for these morphological phenomena to avoid
351 unintentional error. For example, a median section through a small dense cell in the meristem
352 versus a large vacuolated mesophyll cell that may have the same labeling density in the
353 cytoplasm itself, but the large central vacuole would suppress average signal intensity/total cell
354 area. Third, as described herein, plant tissue and wavelength-specific autofluorescence may
355 non-uniformly interfere with fluorescence signal quantification. Fortunately, when fixed emission
356 filters and wavelengths were employed, far red wavelengths were universally more amenable to
357 our tested cytoplasmic and cell wall probes. For greater flexibility, spectral strategies using
358 linear unmixing from reference spectrum can be highly effective and were used successfully to
359 alleviate the impact of autofluorescence in plant studies for quantitative FISH (41). While
360 conventional ISH is semi-quantitative, some FISH-based techniques can be quantitative,
361 including RNAscope® and HCR (24,42). Trivedi et al. (24) used two distinct sets of HCR probes
362 labeled with spectrally separated fluorophores for the same mRNA targets and demonstrated

363 that the two fluorescent signals are highly correlated in a linear relationship with an intercept of
364 zero. Using a homozygous and heterozygous mouse embryo for a known gene, with the
365 expectation that this gene will show 2:1 expression ratio, HCR showed approximately a two-fold
366 difference in mRNA abundance, suggesting that HCR was quantitative (24). Further study and
367 optimization will be required to determine if such quantitative approaches described in whole-
368 mount or cell culture animal systems will translate to sectioned plant protocols.

369 **CONCLUSIONS**

370 HCR FISH has emerged as a novel technique to map the spatial expression patterns of multiple
371 genes concurrently. To apply this method in embedded plant tissues, we used *Arabidopsis*
372 seedlings and *Setaria* inflorescence as our test systems with FFPE and methacrylate de-
373 embedded plant sections. We found these preparations to be compatible with HCR and
374 immunolabeling as well as correlative FESEM studies. In our approach working with sections,
375 omitting proteinase K treatment did not notably affect signal detection and adequately preserved
376 cellular structure. As expected, methacrylate sections produced much better cellular
377 morphology at high resolution compared with paraffin, but working with sections that were often
378 an order of magnitude thinner, required strategies to improve detection and sensitivity,
379 especially with HCR. Despite some compromise in morphology with de-embedded methacrylate
380 sections, adequate ultrastructure of the plant cells was possible after HCR and immunolabeling
381 with thinner slices but was dependent on tissue and imaging conditions. As noted herein,
382 numerous sources and patterns of plant autofluorescence can confound HCR and other affinity
383 probe localization studies without careful assessment and adjustments to experimental design
384 and/or technological strategies. However, several solutions, including judicious choice of
385 fluorophore with labeled probes, leveraging available detection wavelengths, spectral unmixing
386 strategies, instrument configuration and detector choice can help alleviate the problems. This
387 work will serve as a useful basis for future improvements in labeling amplification, fixation,

388 resin/resinless sectioning, multiplexing and potentially signal quantification. Our approach
389 enables studying the localization of multiple RNAs, other affinity probes and the potential for cell
390 pathways combined with cell ultrastructure to be assessed in plant systems as well as other
391 organisms.

392 **MATERIALS AND METHODS**

393 **Reagents and solutions**

394 Reagents for tissue preparation:

395 Diethylpyrocarbonate (DEPC, Bioworld, Cat. No. 1609-47-8, Dublin, OH, USA) H_2O: Add DEPC
396 in milli-Q dH_2O to a final concentration of 0.1%, stir overnight in a fume hood, and autoclave for
397 20 min.

398 10x phosphate buffered saline (PBS) in DEPC H_2O: 1.37 M sodium chloride (NaCl), 27 mM
399 Potassium Chloride (KCl), 43 mM Sodium Phosphate Dibasic (Na_2HPO_4), and 14mM Potassium
400 Phosphate Monobasic (KH_2PO_4) in DEPC H_2O, pH 7.3.

401 16% (w/v) paraformaldehyde (PFA) (Electron Microscopy Sciences, Cat. No. 15710, Hatfield,
402 PA, USA).

403 0.2 M PHEM buffer (Electron Microscopy Sciences, Cat. No. 11165, Hatfield, PA, USA): 120
404 mM PIPES, 50 mM HEPES, 20 mM EGTA, 4 mM $MgCl_2$, pH 7.2.

405 PFA fixative in PBS: 4% (w/v) PFA and 0.1% (v/v) Tween-20 in 0.1 M PBS.

406 PFA fixative in PHEM: 4% (w/v) PFA in 0.1 M PHEM.

407 Histo-Clear® (National Diagnostics, Cat. No. HS-200, Atlanta, GA, USA).

408 Paraffin wax chips (Paraplast Plus, Cat. No. 39502004, McCormick Scientific, Saint Louis, MO,
409 USA).

410 Embedding Ring (Simport Scientific. Cat. No. M460, Quebec, Canada)

411 Base molds (Fisher Scientific. Cat. No. 22-363-553, Hampton, NH, USA)

412 Methyl Methacrylate/Butyl Methacrylate (Electron Microscopy Sciences, Cat. Nos. 18800 &
413 12100, Hatfield, PA, USA): Mix Methyl Methacrylate: Butyl Methacrylate in a 1:3 ratio. For final
414 polymerization, under a stream of nitrogen gas, 0.5% (w/v) benzoin ethyl ether (Electron
415 Microscopy Sciences, Cat. No. 11280, Hatfield, PA, USA) was added to the methacrylate
416 monomer solution and mixed for at least 10 min, avoiding the introduction of oxygen in the resin,
417 which can inhibit polymerization.

418 Vectabond® (Vector Laboratories, Cat. No. SP–1800, Newark, CA, USA)

419 <u>Reagents for HCR:</u>

420 Ethanol series: 30%, 50%, 70% and 90% ethanol diluted in DEPC H_2O.

421 Acetone (Sigma, Cat. No. 179124, St. Louis, MO, USA)

422 Nuclease free water (ThermoFisher, Cat. No. AM9930, Waltham, MA USA)

423 Deionized formamide (EMD Millipore, Cat. No. S4117, Burlington, MA, USA)

424 EDTA, 0.5M (VWR, Cat. No. 97062-654, Radnor, PA, USA))

425 0.2% glycine in PBS: Make 10% (w/v) Glycine in 1x PBS, dilute to a final concentration of 0.2%
426 glycine with 1x PBS.

427 20x saline-sodium citrate (SSC) in DEPC H_2O: 3 M NaCl, 0.3 M sodium citrate in DEPC H_2O.

428 Probe Hybridization Buffer (Molecular Instruments, Los Angeles, CA, USA): 30% formamide, 5x
429 SSC, 9 mM citric acid (pH 6), 0.1% Tween-20, 50 µg/ml heparin, 1X Denhardt's solution and
430 10% dextran sulfate.

431 50% Probe Wash Buffer: Dilute Probe Wash Buffer (Molecular Instruments, Los Angeles, CA,
432 USA) in 5x SSCT (0.1%Tween-20). The final concentrations are 15% formamide, 750mM
433 sodium chloride, 75mM sodium citrate, 4.5 mM citric acid (pH 6), 0.1% Tween-20 and 25 µg/ml
434 heparin.

435 Amplification Buffer (Molecular Instruments, Los Angeles, CA, USA): 5x SSCT (0.1%Tween-20)
436 and 10% dextran sulfate.

437 Hairpins (H1 and H2) with conjugated fluorophores (Alexa Fluor 488/546/647) for each system
438 used (B1 – B5, Molecular Instruments, Los Angeles, CA, USA)

439 Oligonucleotide Probe Sets (IDT, Coralville, IA, USA or Molecular Instruments)

440 <u>Solution used for probe PAGE purification and in vitro assays:</u>

441 Formamide loading buffer: deionized formamide (Sigma-Aldrich, Cat No. F9037, Burlington, MA,
442 USA) with 10 mM EDTA

443 Elution buffer: 500 mM ammonium acetate, 10 mM magnesium acetate, 1 mM EDTA, 0.1%
444 SDS, pH 8.0

445 1x TBE buffer: 89 mM Tris base, 89mM boric acid, 2mM EDTA

446 GelRed (Phenix Research Products. No.C755G19, Swedesboro, NJ, USA)

447 RedSafe (Bulldog Bio, Woburn, MA, USA)

448 100 bp Plus and 1 kb Plus DNA ladders (Goldbio, Saint Louis, MO, USA)

449 6X loading buffer (New England Biolabs, Ipswich, MA, USA)

450 Reagents for Immunolabelling:

451 Rabbit anti-actin polyclonal antibody (Agrisera, Cat. No. AS 13 2640, Vannas, Sweden)

452 LM19 rat anti-homogalacturonan monoclonal antibody (Agrisera, Cat. No. AS18 4191, Vannas,
453 Sweden)

454 Donkey anti-rabbit IgG DyLight 650 (Agrisera, Cat. No. AS12 2329, Vannas, Sweden)

455 Goat anti-rat IgG Alexa Fluor 647 (Invitrogen, Cat. No. A21247, Vannas, Sweden)

456 Blocking buffer: 5% bovine serum albumin (BSA) (Sigma-Aldrich, Cat. No. A8577, Saint Louis,
457 MO, USA) in PBST (0.1% Tween-20)

458 Reagents for fluorescent imaging:

459 Calcofluor White solution: 5 mM Calcofluor White (Biotium, Cat. No. 29067, Fremont, CA, USA)
460 to a final concentration of 50 μM in water.

461 DAPI (4′,6-diamidino-2-phenylindole) solution: Dilute 1 mg/ml DAPI (ThermoFisher, Cat. No.
462 62248, Rockford, IL, USA) to a final concentration of 0.5 μg/ml in 1x PBST (0.1% Tween-20).

463 SlowFade™ Glass antifade mountant, 1.52 refractive index (Thermo Fisher Invitrogen, Cat. No.
464 S36917, Waltham, MA, USA)

465 Two-component silicone-glue Twinsil® (Picodent, Reagent A Cat. No. 32002.42011-12,

466 Reagent B Cat. No. 34001.02014-06 Wipperfurth, Germany): Mix the two components in 1:1

467 ratio.

468 Reagents for FESEM:

469 2% Osmium tetroxide (Electron Microscopy Sciences, Cat. No. 19110, Hatfield, PA, USA):
470 dissolve two 1-g ampules in 100 ml of water.

471 0.1% $KMnO_4$ in 0.1 N H_2SO_4: Add 0.01g $KMnO_4$ (Sigma-Aldrich, Cat. No. 223468, St. Louis,
472 MO, USA) in 10 mL 0.1 N H_2SO_4 (Fisher Scientific, Cat. No. SA818-500, Pittsburg, PA, USA).
473 This solution was filtered with a 0.2 µm PES filter (Whatman UnifloTM, Cytiva,
474 Buckinghamshire, UK) prior to use.

475 1% (w/v) methanolic uranyl acetate: Add 1g uranyl acetate (SPI Supplies, Cat. No. 02624-AB,
476 West Chester, PA, USA) to 100 mL methanol (Electron Microscopy Sciences, Cat. No. 18510,
477 Hatfield, PA, USA): This solution was filtered with a 0.2 µm PES filter prior to use.

478 Sato's lead solution: Add 0.20 g anhydrous lead citrate (Electron Microscopy Sciences, Cat. No.
479 17800, Hatfield, PA, USA), 0.15 g lead nitrate (Electron Microscopy Sciences, Cat. No. 17900,
480 Hatfield, PA, USA), 0.15 g lead acetate (Electron Microscopy Sciences, Cat. No. 17600,
481 Hatfield, PA, USA), 1.00 g sodium citrate (Electron Microscopy Sciences, Cat. No. 21140,
482 Hatfield, PA, USA) and 41.0 mL distilled water in a 50 mL volumetric flask, mix well and adjust
483 pH with 9 mL 1N NaOH (Electron Microscopy Sciences, Cat. No. 21160, Hatfield, PA, USA).
484 This solution was filtered with a 0.2 µm PES filter prior to use.

485 **Equipment and Supplies**

486 - Leica EG1150 tissue embedder
487 - Leica RM2255 rotary microtome
488 - Incubators set to 37°C and 60°C
489 - Slide warmer
490 - Probe-On Plus Slides (Fisher Scientific, Pittsburgh, PA, USA)

491 • Adhesive treated coverslips: Glass coverslips (No. 1.5, 22mm x 22mm) were coated with
492 Vectabond® (Vector Laboratories, Newark, CA, USA) following the manufacturer's
493 recommendations and allowed to dry.
494 • EMS UVC3 Ultraviolet Cryo Chamber (Electron Microscopy Sciences, Cat. No. 70445-
495 10, Hatfield, PA, USA)
496 • BEEM capsules (Size 00, 8mm I.D, Electron Microscopy Sciences, Cat. No. 70000-B)
497 • DiATOME Ultra 45°, 2.0 mm Diamond knife (Diatome, Quakertown, PA, USA
498 • Leica UltraCut UCT ultramicrotome (Leica Microsystems, Vienna, Austria)
499 • Azure Biosystems C6 Gel Scanner (Dublin, CA, USA)
500 • Heat block set to 95°C
501 • Vacuum desiccator
502 • Sealed humid container (This can be made in-house from many types of plastic
503 containers which have a sealable lid. Elevating the glass slides and coverslips off the
504 bottom with spacers helps to avoid the solutions wicking away from the sections into the
505 moist paper towels below)
506 • Microfuge
507 • NanoDrop spectrophotometer
508 • Glass Coplin jars
509 • Slide mailers
510 • Coverslip mini-rack (Thermo Fisher, Cat. No. C14784, Waltham, MA, USA)
511 • 50 mLbeakers
512 • Parafilm (Bemis, IL, USA)
513 • Leica TCS SP8 confocal laser scanning microscope (Leica Microsystems, Wetzler,
514 Germany)
515 • ZEISS Elyra 7 super-resolution microscope with Lattice SIM² (Zeiss, Jena, Germany)

516 • ZEISS Merlin field emission scanning electron microscope with ATLAS 5 Software
517 (Zeiss, Oberkochen, Germany)
518 • ZEISS LSM980 confocal microscope with Quasar spectral detector (Zeiss, Jena,
519 Germany)

520 **Plant Materials**

521 *Setaria viridis* (accession A10) seeds were sown in Jolly Gardener soil, kept at 4°C in the dark
522 for 2 weeks to break dormancy, then grown in a growth chamber maintaining 12 h/12 h
523 (day/night) photoperiod and 31°C/22°C (day/night) temperatures, 50% humidity and 350
524 μmol/m^2/sec light intensity. *Arabidopsis thaliana* (Col-0) seeds were sterilized and sown on ½
525 strength Murashige & Skoog medium, 1% sucrose and 0.8% agar (pH 5.8) in a growth chamber
526 with a 16 h/8 h day/night (22°C/19°C) regime, 50% humidity and 200 μmol/m^2/sec light intensity.

527 **HCR and Immunofluorescence Sample Processing and Imaging Workflow**

528 We encapsulated the most complete scenario for labeling and imaging workflows of multiple
529 probe classes in Figure 8. The vast majority of the processing time involves sample fixation and
530 embedment and generating tissue sections. Immunolabelling and correlative FESEM can follow
531 HCR and are optional. Probe sets that produce relatively low signals (below the detection limit
532 of laser scanning confocal microscopy (LSCM)) can be successfully imaged with high quantum
533 efficiency imaging modalities. The details of the experimental workflow are as follows below:

534 **HCR Probe Set Design**

535 Custom split initiator probe sets may be designed and ordered directly from Molecular
536 Instruments or manually designed based on the specifications described in (23) as follows. A
537 list of prospective 22 nt oligomer probes was generated using an online probe design tool (43),
538 and their locations were manually mapped onto the target sequence using the free plasmid DNA

539 mapping software SnapGene Viewer. Regions of the target mRNA where two 22 nt probes were
540 located in close proximity (20 nt or less) were considered as prime locations for generating HCR
541 probe pairs. The sequences of the probes were then manually extended to 25 nt each, and
542 their locations were adjusted so that the pairs were separated by 2 nt of either G and/or C and
543 had predicted melting temperatures of 35-60°C for each probe. This process was repeated until
544 probe pairs were spaced along the entire CDS and 3'UTR of the target mRNA. The probe
545 sequences were confirmed to be specific using NCBI nucleotide BLAST. Final probe sets were
546 composed of 6-12 probe pairs (12-24 probes). One of the five unique initiator sequences (B1-
547 B5) (23) was chosen for each target mRNA probe set. The 5' or 3' half of the 36 nt initiator
548 sequence followed by a 2 nt spacer was added to either the 5' end of the odd numbered anti-
549 sense probe sequence, or the 3' end of the even numbered anti-sense probe sequence,
550 respectively, resulting in a final HCR probe length of 45 nt. The commercially generated
551 oligomers with standard desalting were dissolved to 100 µM in nuclease free water. The
552 individual stock probe solutions were then mixed and diluted to 2 µM/probe in nuclease free
553 water. Initiators and full sequences of the probe sets used in this work are shown in Table S1.

554 **HCR Probe PAGE Purification (1 day)**

555 Probe sets which showed non-specific puncta on an initial HCR experiment were PAGE purified
556 as follows. An 8% polyacrylamide (8 M urea, 1x TBE) solution was mixed, degassed for 15 min
557 under vacuum and polymerized with 0.05% fresh ammonium persulfate and 0.001% TEMED
558 and poured into two 1mm Bio-Rad Protean II mini gels. The gels were pre-run at 200V for 30
559 min in 1x TBE buffer. 100 µg total of the odd numbered probe stocks were mixed and diluted
560 with an equal volume of formamide loading buffer, heated to 95°C for 2 min, then snap cooled
561 on ice. The entire volume of the odd numbered probe mixture was loaded equally into the wells
562 of one gel along with a single well of formamide loading buffer containing 0.1% xylene cyanole
563 FF and 0.1% bromophenol blue to serve as size markers. The even numbered probes were

564 prepared in a similar fashion and loaded into the second gel and both were run at 200V until the
565 bromophenol blue reached the bottom of the gel. The edges of the gels were notched at the
566 locations of the two dye bands (xylene cyanole 75 bp, bromophenol blue 19bp), stained with
567 GelRed (Phenix Research Products), imaged under UV and the large 45 nt band isolated,
568 minced and loaded into 0.5 ml microfuge tubes. The tubes were perforated by a sharp needle
569 five times, inserted into 1.5 mL microfuge tubes, and spun at 10,000 g until the gel had been
570 crushed into the larger tubes. Next, 400 µl of elution buffer was added to the gel pieces and
571 incubated at 37°C overnight. The elution buffer with DNA was removed from the gel pieces, and
572 the DNA precipitated with 1/10th volume of 3 M sodium acetate and 2.5 volumes of 100%
573 ethanol at -20℃ for 30 min. The DNA was pelleted at 10,000 x g for 30 min at 4℃, and the
574 supernatant was removed. The pellet was washed in 70% ethanol at RT, dried at RT for 15 min
575 and dissolved in nuclease free water. Probe concentrations were determined by a NanoDrop
576 spectrophotometer.

577 **In-vitro HCR Assay (optional)**

578 A custom 52nt oligo, corresponding to the sense strand of the CAB1 mRNA targeted by probe 1
579 and 2, was generated commercially (IDT, Coralville, IA) along with the 36 nt system B2 initiator
580 sequence (Table S1) (23). The B2 hairpins, conjugated to Alexa Fluor 546, were heated to 95°C
581 for 90 sec then allowed to cool at RT in the dark for 30 min. The target, initiator and probes
582 were heated to 95°C for 90 sec then snap cooled on ice. Next, 12 µl reactions were then set up
583 in 5X SSCT (0.1% Tween-20) with the following final concentrations: System B2 hairpin H1 and
584 H2 each 125 nM, B2 initiator 5 nM, target oligonucleotide 10 nM, split initiator probes 1 and 2 at
585 10 nM each. The reactions were incubated at 25°C for 4 hr. 2µl of 6X loading buffer (New
586 England Biolabs, Ipswich, MA) was added to each reaction and then loaded onto a 1%
587 agarose/TBE gel along with 5 µl each of 100 bp Plus and 1 kb Plus DNA ladders (Goldbio, Saint
588 Louis, MO). The gel was run at 105V for 45 min and stained with 1X RedSafe (Bulldog Bio,

589 Woburn, MA) in TBE for 30 min. The gel was imaged with an Azure Biosystems C6 Gel Scanner
590 (Dublin, CA) with peak excitation/emission wavelengths of 530/572 nm.

591 **Fixation, Embedding and sectioning (5-6 Days)**

592 Once HCR Probes are generated and purified, all subsequent steps below provide details from
593 specimen fixation until image processing as outlined for the HCR Workflow (Fig.8).

594 After 17 days in the growth chamber, *Setaria* panicles were dissected under a stereo
595 microscope. Panicles were then fixed in PFA fixative in PBS under vacuum for 10 min on ice,
596 then overnight in fresh fixative at 4°C. All processing steps were conducted in standard 20 mL
597 glass scintillation vials. After washing two times in 1x PBS for 30 min each on ice, the tissue
598 was processed through a standard paraffin embedding protocol. The samples were dehydrated
599 through a graded series of ethanol (30%, 50%, 70%, 95%, 100%, 100%) for 1 hr each on ice,
600 followed by 100% ethanol overnight at 4°C. The ethanol was gradually replaced using 1 hr
601 incubations in 25%, 50%, 75% Histo-Clear® diluted in ethanol at 22°C (RT), followed by three
602 times in 100% Histo-Clear®. Then the vial was filled with paraffin wax chips and incubated
603 overnight at RT, followed by 2 h incubation at 42°C and at 60°C until the wax chips completely
604 melted. The solution was replaced with fresh 100% melted paraffin at 60°C six times over 2-3
605 days. The samples were then embedded in paraffin using a Leica EG1150 tissue embedder,
606 allowed to harden and stored at 4°C. Next, 10µm longitudinal sections were cut using a Leica
607 RM2255 rotary microtome, placed on Probe-On Plus Slides, briefly stretched on a droplet of
608 water and allowed to dry overnight on a 37°C slide warmer. Slides were stored desiccated at
609 4°C in the dark.

610 Three-day-old *Arabidopsis* seedlings were fixed in PFA fixative in PHEM buffer at 4°C.
611 Following the ethanol dehydration series, half the seedlings were processed in paraffin (see
612 above), while the remaining samples were embedded in methacrylate resin. The seedlings were

613 infiltrated in 25%, 50%, 75% methacrylate (1:3 methyl methacrylate: n-butyl methacrylate)
614 diluted in ethanol for 2 h each, followed by two changes of 100% methacrylate for 24 h each at
615 RT. The seedlings were then embedded in methacrylate with benzoin ethyl ether under a
616 constant stream of nitrogen gas in BEEM capsules and polymerized under UV radiation for 48 h
617 at -20°C using a UVC Cryo Chamber filled with dry ice. Capsules were removed and the blocks
618 allowed to cure in a fume hood at RT until solid. 0.5-1.5 µm semi-thin sections were cut using a
619 diamond knife and Leica UltraCut UCT ultramicrotome. The sections were stretched with
620 chloroform vapors and transferred to adhesive-treated coverslips to allow drying at 42°C for 1h.
621 Coverslips were stored at 4°C in the dark. The best experimental results were obtained using
622 sections cut within ~2 weeks of the HCR procedure.

623 **HCR (2.5 days)**

624 Paraffin sections on slides were incubated for 2 x 10 min in Histo-Clear® in glass Coplin jars to
625 remove the wax. Methacrylate sections on coverslips were de-embedded for 10 min in acetone
626 using a coverslip mini-rack in a 50 mL glass beaker. For all remaining steps, the paraffin and
627 methacrylate sections were treated in parallel. Wash steps for the paraffin sections were
628 conducted in plastic slide mailers. Methacrylate sections continued to be processed by moving
629 the coverslip mini-rack through a series of glass beakers with the appropriate solutions.
630 Sections were rehydrated in a decreasing graded series of ethanol (100, 90, 70, 50 and 30%)
631 for 2 min each, followed by two washes in 1x PBS for 2 min each. Sections were then incubated
632 in 0.2% glycine in PBS for 5 min, washed in 1x PBS twice for 2 min each and dehydrated in a
633 series of increasing graded ethanol for 2 min each, ending in 2 changes of 100% ethanol for 5
634 min each. Sections were air dried in a vacuum for 1 h at RT. This pre-treatment regime
635 eliminates several steps commonly found in conventional *in situ* hybridization protocols
636 including proteinase K digestion, re-fixation and triethanolamine (TEA) incubation. These steps
637 had no notable effect on HCR labeling results and eliminating them resulted in a shorter and

638 simpler protocol as well as reduced extraction that would impact morphology and some antigens
639 for immunolabeling.

640 Custom-designed split initiator oligonucleotide probes were diluted in the hybridization buffer at
641 a final concentration of 20 nM/probe. The probe solution (125 µL for slides and 75 µL for
642 coverslips) was pipetted over the sections and covered with a piece of Parafilm which had been
643 cut to a slightly smaller dimension than the slides or coverslips. The slides and coverslips were
644 incubated at 37°C overnight in a moist chamber. The hybridization solution was drained away,
645 and the slides and coverslips were washed in 50% Probe Wash Buffer at 37°C for 15 min,
646 followed by 2x SSCT (0.1% Tween-20) incubation at 37°C for 15 min and a final 15 min wash in
647 5x SSCT (0.1% Tween-20) at RT.

648 Each pair of fluorophore-conjugated hairpins (H1 and H2) needed for an experiment was
649 pipetted into separate microfuge tubes and heated to 95°C for 90 sec in a heat block, then
650 allowed to refold at RT for 30 min in the dark. The tubes were then spun down and the hairpins
651 were added to Amplification Buffer at a final concentration of 60 nM. The hairpin buffer was then
652 pipetted over the sections, covered with Parafilm, and incubated in a moist chamber overnight
653 at RT in the dark. The hairpin buffer was drained off, and the slides and coverslips were washed
654 3 x 10 min in 5x SCCT.

655 **Immunolabeling (0.5 day)**

656 In experiments where immunolabeling was performed after HCR, the sections were incubated in
657 blocking buffer for 1 h at RT in a moist chamber. Primary antibodies (125 µL per slide and 75 µL
658 per coverslip) were diluted in blocking buffer (1:15 dilution for LM19 and 1:200 dilution for anti-
659 actin) and incubated on the sections for 1 h in the dark at RT in a moist chamber. The primary
660 antibody solution was drained off and the sections were washed 3 x 15 min in blocking buffer.
661 Fluorophore-conjugated secondary antibodies were diluted 1:1000 in blocking buffer and

662 incubated on the sections for 1 h at RT in the dark in a moist chamber. The secondary antibody
663 solution was drained off and the sections and coverslips were washed 3 x 15 min in PBST.

664 **Cell Wall and Nuclear Staining (~0.5 h)**

665 After HCR (and immunolabeling), samples were stained to differentiate individual cells. Cell
666 walls were stained with Calcofluor White diluted 1:200 in water for 20 min at RT in the dark in a
667 moist chamber. Nuclei were stained with DAPI solution for 30 min at RT in the dark in a moist
668 chamber. The slides and coverslips were washed in 1x PBS, quickly dipped into water, mounted
669 using SlowFade™ Glass antifade mountant, and sealed with Twinsil. The samples can be
670 imaged immediately or stored at 4°C in the dark for up to 2 weeks without appreciable loss of
671 HCR signal or specificity.

672 **Imaging and Image Processing**

673 All the laser scanning confocal microscope images were taken with a Leica TCS SP8 with white
674 light lasers using the Leica Las X software and the following objectives: 63x/1.2 HC PL APO
675 CS2 water immersion, 40x/1.1 PL APO CS2 water immersion and 20x/0.7 HC PL APO air lens.
676 Images were taken at 1024 x 1024 pixels with a bit depth of 12. Calcofluor White was excited
677 using the 405 nm diode laser line and collected at 410-473 nm. Alexa Fluor 488 was excited
678 using the 488 nm laser line and collected at 508-552 nm. Alexa Fluor 546 was excited using the
679 514 nm laser line and collected at 571-628 nm. Alexa Fluor 647 and DyLight 650 were excited
680 with the 664 nm laser line and collected at 662-748 nm. Spectral imaging was performed using
681 a Zeiss C-Apochromat 40X/1.2 W Korr FCS objective on a ZEISS LSM980 equipped with a
682 Quasar spectral detector using simultaneous laser excitation with 405 nm, 488 nm, 561 nm and
683 640 nm diode laser lines and covering 411-694 nm with 32 channels at 9 nm GaAsP-PMT
684 detector windows. Images were acquired at 16 Bit, 69 nm x-y pixel resolution, 3091 x 3091 pixel
685 frame size and brightness levels were adjusted uniformly for visualization using Fiji (44) and the

686 images were converted to TIFF format for final figure assembly. Experimental and negative
687 control images were taken using identical microscope settings and displayed with matching
688 black and white levels with experimental samples in Fiji. Lattice SIM super-resolution images
689 were taken with a Zeiss Elyra 7 inverted microscope running the Zen Black 3.0 software
690 package and a 40x/1.4 Plan Apochromat DIC M27 oil immersion objective. Consecutive z-stack
691 images were taken at 1024x1024 pixel frame size and at 16 Bit. Voxel scaling was 0.0099 x
692 0.099 x 0.329 μm. Calcofluor White was excited with 405-nm and ACT7 with 488-nm lasers
693 sequentially in fast frame mode. Respective emissions were detected using the CMOS camera
694 and BP420-480 + BP 495-550 filter. The Zeiss SIM^2 deconvolution processing module was used
695 to process the images and option “scale to raw image” was selected to retain original relative
696 signal intensities.

697 **Staining coverslips for SEM (~3 h)**

698 This protocol was modified from (45). Coverslips were placed section-side up on a petri dish
699 and rinsed well with double-distilled water (ddH_2O) on a benchtop shaker at low speed for 15
700 mins. Then in a fume hood, the coverslips were floated section-side down on 200µL droplets of
701 2% Osmium tetroxide for 1 hour and rinsed with ddH_2O for 10 mins. Coverslips were then
702 floated on droplets of 0.1% $KMnO_4$ dissolved in 0.1N H_2SO_4 for 1 min and then rinsed with
703 ddH_2O for 5-10 mins. Drops of filtered 1% methanolic Uranyl Acetate (UA) were placed in a petri
704 dish lined with parafilm and the coverslips were floated on the UA droplets for 30 mins. Next, the
705 coverslips were rinsed by floating on drops of methanol for 5 mins and were allowed to dry
706 before staining with lead. The lead staining chamber was prepared by adding NaOH pellets in a
707 petri dish and the coverslips were floated on drops of filtered Sato's lead solution (46) for 1 min.
708 Finally, coverslips were then rinsed using degassed ddH_2O and excess water was carefully
709 blotted dry and coverslips were allowed to air dry.

710 **SEM imaging**

711 The dried coverslips with sections facing up were mounted onto 25mm aluminum pin stubs with
712 double-sided adhesive carbon tabs and then conductive silver paint was applied connecting the
713 aluminum stub to the top edge of the coverslip surface, ensuring a conductive trail. After the
714 conductive paint dried, the entire coverslip was carbon coated prior to imaging. A ZEISS Merlin
715 was used at 3kV and scanned at 50 nm or 5 nm pixel resolutions and 8 Bit depth with back-
716 scatter electrons detector and with FIBICS ATLAS 5 (v5.3.5.27). Confocal and FESEM images
717 were overlaid using Adobe Photoshop CC 2019, Linear Dodge (Add) was applied to the
718 confocal image to see the combined back-scatter EM and fluorescence image, The Free
719 Transform tool was used to rotate, rescale and align the fluorescence image with the
720 corresponding FESEM image using the plant cell wall (Calcofluor White from the confocal
721 image) and FESEM images for registration features. The Warp non-linear transformation
722 function was used for the final, very minor local cell wall changes that occurred between
723 confocal and FESEM sample treatments.

724 **List of abbreviations**

725 Abscission zone: AZ. *ACTIN7: ACT7*. *CHLOROPHYLL BINDING FACTOR a/b: CAB1*.
726 Digoxygenin: DIG. *ELONGATION FACTOR 1 ALPHA: EF1α*. FFPE: Formalin fixed Paraffin
727 Embedded. Field emission scanning electron microscopy: FESEM. FISH: fluorescent *in situ*
728 hybridization. HCR: hybridization chain reaction. KNOTTED 1: KN1. Nitroblue tetrazolium/ 5-
729 bromo- 4-chloro-3-indolyl-phosphate: NBT/BCIP. PAGE: polyacrylamide gel electrophoresis.
730 Rolling circle amplification: RCA. SHATTERING 1: SH1. Single molecule FISH: smFISH. SIM
731 Structured Illumination Microscopy. Transcription factor: TF. Tyramide signal amplification: TSA.
732 Uranyl acetate: UA.

733 **Declarations**

Availability of data and materials

The transcript sequences of *Setaria viridis SH1* (Sevir.5G293800.1), *KN1* (Sevir.9G107600.1) and MYB26 (5G293800.1) are available on Phytozome 13 (https://phytozome-next.jgi.doe.gov/). The transcript sequences of *Arabidopsis thaliana CAB1* (AT1G29930), *EF1α* (AT1G07940) and *ACT7* (AT5G09810) are available on TAIR (https://www.arabidopsis.org). The probe sequences and images are available within the paper and supplemental materials.

Competing interests

None declared.

Funding

This study was funded by NSF-MCB-EAGER 2130365 to KC, SB, ML and YY, and NSF-IOS 1938086 to EAK.

Authors' contributions

KC, YY, SB, ML, EAK and BM obtained funding. KC, YY, SB, ML designed the research. KC, DH and YY designed the experimental approach. SB, DH and YY prepared the plant materials. DH performed the HCR and Immunolabeling experiments. YY performed the colorimetric ISH. DH, KC and AK acquired the images. JW and KC performed the FESEM. DH, ML and KC performed the image analysis. DH, YY, EAK and KC drafted the manuscript, and all authors discussed the results and edited the manuscript.

Acknowledgements

We gratefully thank the NSF for funding this work (Award # 2130365 to K. Czymmek) and Joanna Porankiewicz-Asplund and Agrisera for providing our tested DyLight Secondary antibodies. We also acknowledge imaging support from the Advanced Bioimaging Laboratory (RRID:SCR_018951) at the Danforth Plant Science Center and usage of the ZEISS Elyra 7

757 Super-Resolution Microscope acquired through an NSF Major Research Instrumentation grant
758 (DBI-2018962). We are also especially appreciative of the expert ZEISS FESEM and ATLAS
759 support from Dr. Sanja Sviben and Washington University Center for Cellular Imaging (WUCCI).

760

761 **REFERENCES**

762 1. Young AP, Jackson DJ, Wyeth RC. A technical review and guide to RNA fluorescence in
763 situ hybridization. PeerJ [Internet]. 2020 Mar 19;8:e8806. Available from:
764 https://peerj.com/articles/8806

765 2. Levsky JM, Singer RH. Fluorescence in situ hybridization: past, present and future. J Cell
766 Sci [Internet]. 2003 Jul 15;116(14):2833–8. Available from:
767 https://journals.biologists.com/jcs/article/116/14/2833/27272/Fluorescence-in-situ-
768 hybridization-past-present

769 3. Jensen E. Technical Review: In Situ Hybridization. Anat Rec [Internet]. 2014 Aug
770 9;297(8):1349–53. Available from:
771 https://anatomypubs.onlinelibrary.wiley.com/doi/10.1002/ar.22944

772 4. Hejátko J, Blilou I, Brewer PB, Friml J, Scheres B, Benková E. In situ hybridization
773 technique for mRNA detection in whole mount Arabidopsis samples. Nat Protoc [Internet].
774 2006 Nov 22;1(4):1939–46. Available from:
775 https://www.nature.com/articles/nprot.2006.333

776 5. Kronenberger J, Desprez T, Höfte H, Caboche M, Traas J. A methacrylate embedding
777 procedure developed for immunolocalization on plant tissues is also compatible with in
778 situ hybridization. Cell Biol Int [Internet]. 1993 Nov 2;17(11):1013–21. Available from:
779 https://onlinelibrary.wiley.com/doi/10.1006/cbir.1993.1031

780 6. Stahl Y, Simon R. mRNA Detection by Whole Mount In Situ Hybridization (WISH) or
781 Sectioned Tissue In Situ Hybridization (SISH) in Arabidopsis. In 2010. p. 239–51.
782 Available from: http://link.springer.com/10.1007/978-1-60761-765-5_16

783 7. Javelle M, Marco CF, Timmermans M. In Situ Hybridization for the Precise Localization of
784 Transcripts in Plants. J Vis Exp [Internet]. 2011 Nov 23;(57). Available from:
785 http://www.jove.com/details.php?id=3328

786 8. Rozier F, Mirabet V, Vernoux T, Das P. Analysis of 3D gene expression patterns in plants
787 using whole-mount RNA in situ hybridization. Nat Protoc [Internet]. 2014 Oct
788 25;9(10):2464–75. Available from: https://www.nature.com/articles/nprot.2014.162

789 9. Zöllner NR, Bezrutczyk M, Laureyns R, Nelissen H, Simon R, Frommer WB. An RNA in
790 situ hybridization protocol optimized for monocot tissue. STAR Protoc [Internet]. 2021
791 Jun;2(2):100398. Available from:
792 https://linkinghub.elsevier.com/retrieve/pii/S2666166721001052

793 10. Raj A, van den Bogaard P, Rifkin SA, van Oudenaarden A, Tyagi S. Imaging individual
794 mRNA molecules using multiple singly labeled probes. Nat Methods [Internet]. 2008 Oct
795 21;5(10):877–9. Available from: https://www.nature.com/articles/nmeth.1253

796 11. Duncan S, Olsson TSG, Hartley M, Dean C, Rosa S. A method for detecting single
797 mRNA molecules in Arabidopsis thaliana. Plant Methods [Internet]. 2016 Dec 5;12(1):13.
798 Available from: http://plantmethods.biomedcentral.com/articles/10.1186/s13007-016-
799 0114-x

800 12. Yang W, Schuster C, Prunet N, Dong Q, Landrein B, Wightman R, et al. Visualization of
801 Protein Coding, Long Noncoding, and Nuclear RNAs by Fluorescence in Situ
802 Hybridization in Sections of Shoot Apical Meristems and Developing Flowers. Plant

803 Physiol [Internet]. 2020 Jan;182(1):147–58. Available from:
804 https://academic.oup.com/plphys/article/182/1/147-158/6116070

805 13. Nobori T, Oliva M, Lister R, Ecker JR. Multiplexed single-cell 3D spatial gene expression
806 analysis in plant tissue using PHYTOMap. Nat Plants [Internet]. 2023 Jun 12;9(7):1026–
807 33. Available from: https://www.nature.com/articles/s41477-023-01439-4

808 14. Wang F, Flanagan J, Su N, Wang L-C, Bui S, Nielson A, et al. RNAscope. J Mol
809 Diagnostics [Internet]. 2012 Jan;14(1):22–9. Available from:
810 https://linkinghub.elsevier.com/retrieve/pii/S1525157811002571

811 15. Choi HMT, Beck VA, Pierce NA. Next-Generation in Situ Hybridization Chain Reaction:
812 Higher Gain, Lower Cost, Greater Durability. ACS Nano [Internet]. 2014 May
813 27;8(5):4284–94. Available from: https://pubs.acs.org/doi/10.1021/nn405717p

814 16. Choi HMT, Schwarzkopf M, Fornace ME, Acharya A, Artavanis G, Stegmaier J, et al.
815 Third-generation in situ hybridization chain reaction: Multiplexed, quantitative, sensitive,
816 versatile, robust. Dev. 2018;145(12):1–10.

817 17. Speel EJM, Hopman AHN, Komminoth P. Tyramide Signal Amplification for DNA and
818 mRNA In Situ Hybridization. In: In Situ Hybridization Protocols [Internet]. New Jersey:
819 Humana Press; p. 33–60. Available from: http://link.springer.com/10.1385/1-59745-007-
820 3:33

821 18. Ke R, Mignardi M, Pacureanu A, Svedlund J, Botling J, Wählby C, et al. In situ
822 sequencing for RNA analysis in preserved tissue and cells. Nat Methods [Internet]. 2013
823 Sep 14;10(9):857–60. Available from: https://www.nature.com/articles/nmeth.2563

824 19. Gyllborg D, Langseth CM, Qian X, Choi E, Salas SM, Hilscher MM, et al. Hybridization-
825 based in situ sequencing (HybISS) for spatially resolved transcriptomics in human and

826 mouse brain tissue. Nucleic Acids Res [Internet]. 2020 Nov 4;48(19):e112–e112.
827 Available from: https://academic.oup.com/nar/article/48/19/e112/5912821

828 20. Bowling AJ, Pence HE, Church JB. Application of a novel and automated branched DNA
829 in situ hybridization method for the rapid and sensitive localization of mRNA molecules in
830 plant tissues. Appl Plant Sci [Internet]. 2014 Apr 3;2(4). Available from:
831 https://bsapubs.onlinelibrary.wiley.com/doi/10.3732/apps.1400011

832 21. Munganyinka E, Margaria P, Sheat S, Ateka EM, Tairo F, Ndunguru J, et al. Localization
833 of cassava brown streak virus in Nicotiana rustica and cassava Manihot esculenta
834 (Crantz) using RNAscope® in situ hybridization. Virol J [Internet]. 2018 Dec 14;15(1):128.
835 Available from: https://virologyj.biomedcentral.com/articles/10.1186/s12985-018-1038-z

836 22. Solanki S, Ameen G, Zhao J, Flaten J, Borowicz P, Brueggeman RS. Visualization of
837 spatial gene expression in plants by modified RNAscope fluorescent in situ hybridization.
838 Plant Methods [Internet]. 2020 Dec 15;16(1):71. Available from:
839 https://plantmethods.biomedcentral.com/articles/10.1186/s13007-020-00614-4

840 23. Choi HMT, Schwarzkopf M, Fornace ME, Acharya A, Artavanis G, Stegmaier J, et al.
841 Third-generation in situ hybridization chain reaction: multiplexed, quantitative, sensitive,
842 versatile, robust. Development [Internet]. 2018 Jun 15;145(12). Available from:
843 https://journals.biologists.com/dev/article/145/12/dev165753/48466/Third-generation-in-
844 situ-hybridization-chain

845 24. Trivedi V, Choi HMT, Fraser SE, Pierce NA. Multidimensional quantitative analysis of
846 mRNA expression within intact vertebrate embryos. Development [Internet]. 2018 Jan
847 1;145(1). Available from:
848 https://journals.biologists.com/dev/article/145/1/dev156869/48765/Multidimensional-
849 quantitative-analysis-of-mRNA

850 25. Huang T, Guillotin B, Rahni R, Birnbaum KD, Wagner D. A rapid and sensitive, multiplex,
851 whole mount RNA fluorescence in situ hybridization and immunohistochemistry protocol.
852 Plant Methods [Internet]. 2023 Nov 22;19(1):131. Available from:
853 https://plantmethods.biomedcentral.com/articles/10.1186/s13007-023-01108-9

854 26. Oliva M, Stuart T, Tang D, Pflueger J, Poppe D, Jabbari JS, et al. An environmentally
855 responsive transcriptional state modulates cell identities during root development. bioRxiv
856 [Internet]. 2022;2022.03.04.483008. Available from:
857 https://www.biorxiv.org/content/10.1101/2022.03.04.483008v2%0Ahttps://www.biorxiv.org
858 /content/10.1101/2022.03.04.483008v2.abstract

859 27. Lherminier J, Bonfiglioli RG, Daire X, Symons RH, Boudon-Padieu E.
860 Oligodeoxynucleotides as probes forin situhybridization with transmission electron
861 microscopy to specifically localize phytoplasma in plant cells. Mol Cell Probes [Internet].
862 1999 Feb;13(1):41–7. Available from:
863 https://linkinghub.elsevier.com/retrieve/pii/S0890850898902134

864 28. Motte PM, Loppes R, Menager M, Deltour R. Three-dimensional electron microscopy of
865 ribosomal chromatin in two higher plants: a cytochemical, immunocytochemical, and in
866 situ hybridization approach. J Histochem Cytochem [Internet]. 1991 Nov 5;39(11):1495–
867 506. Available from: http://journals.sagepub.com/doi/10.1177/39.11.1918926

868 29. Harris N, Croy RRD. Localization of mRNA for pea legumin:In situ hybridization using a
869 biotinylated cDNA probe. Protoplasma [Internet]. 1986 Feb;130(1):57–67. Available from:
870 http://link.springer.com/10.1007/BF01283331

871 30. Warren KC, Coyne KJ, Waite JH, Cary SC. Use of Methacrylate De-embedding Protocols
872 for In Situ Hybridization on Semithin Plastic Sections with Multiple Detection Strategies. J
873 Histochem Cytochem [Internet]. 1998 Feb 26;46(2):149–55. Available from:

http://journals.sagepub.com/doi/10.1177/002215549804600203

31. Mueller M, Wacker K, Hickey WF, Ringelstein EB, Kiefer R. Co-Localization of Multiple Antigens and Specific DNA. Am J Pathol [Internet]. 2000 Dec;157(6):1829–38. Available from: https://linkinghub.elsevier.com/retrieve/pii/S0002944010648225

32. Yu Y, Hu H, Doust AN, Kellogg EA. Divergent gene expression networks underlie morphological diversity of abscission zones in grasses. New Phytol [Internet]. 2020 Feb 28;225(4):1799–815. Available from: https://nph.onlinelibrary.wiley.com/doi/10.1111/nph.16087

33. Jackson D, Veit B, Hake S. Expression of maize KNOTTED1 related homeobox genes in the shoot apical meristem predicts patterns of morphogenesis in the vegetative shoot. Development [Internet]. 1994 Feb 1;120(2):405–13. Available from: https://journals.biologists.com/dev/article/120/2/405/38273/Expression-of-maize-KNOTTED1-related-homeobox

34. Bolduc N, Yilmaz A, Mejia-Guerra MK, Morohashi K, O'Connor D, Grotewold E, et al. Unraveling the KNOTTED1 regulatory network in maize meristems. Genes Dev [Internet]. 2012 Aug 1;26(15):1685–90. Available from: http://genesdev.cshlp.org/lookup/doi/10.1101/gad.193433.112

35. Brewer PB, Heisler MG, Hejátko J, Friml J, Benková E. In situ hybridization for mRNA detection in Arabidopsis tissue sections. Nat Protoc [Internet]. 2006 Aug 9;1(3):1462–7. Available from: https://www.nature.com/articles/nprot.2006.226

36. Donaldson L. Autofluorescence in Plants. Molecules [Internet]. 2020 May 21;25(10):2393. Available from: https://www.mdpi.com/1420-3049/25/10/2393

37. De Mazière A, van der Beek J, van Dijk S, de Heus C, Reggiori F, Koike M, et al. An

897 optimized protocol for immuno-electron microscopy of endogenous LC3. Autophagy
898 [Internet]. 2022 Dec 2;18(12):3004–22. Available from:
899 https://www.tandfonline.com/doi/full/10.1080/15548627.2022.2056864

900 38. Mansfield JR, Gossage KW, Hoyt CC, Levenson RM. Autofluorescence removal,
901 multiplexing, and automated analysis methods for in-vivo fluorescence imaging. J Biomed
902 Opt [Internet]. 2005;10(4):041207. Available from:
903 http://biomedicaloptics.spiedigitallibrary.org/article.aspx?doi=10.1117/1.2032458

904 39. Huang K, Demirci F, Batish M, Treible W, Meyers BC, Caplan JL. Quantitative, super-
905 resolution localization of small RNAs with sRNA-PAINT. Nucleic Acids Res.
906 2020;48(16):e96.

907 40. McDowell JM, An Y, Huang S, McKinney EC, Meagher RB. The Arabidopsis ACT7 Actin
908 Gene Is Expressed in Rapidly Developing Tissues and Responds to Several External
909 Stimuli. Plant Physiol [Internet]. 1996 Jul 1;111(3):699–711. Available from:
910 https://academic.oup.com/plphys/article/111/3/699/6070322

911 41. Huang K, Batish M, Teng C, Harkess A, Meyers BC, Caplan JL. Quantitative
912 Fluorescence In Situ Hybridization Detection of Plant mRNAs with Single-Molecule
913 Resolution. In 2020. p. 23–33. Available from: http://link.springer.com/10.1007/978-1-
914 0716-0712-1_2

915 42. Huang G, Eckrich S. Quantitative Fluorescent in situ Hybridization Reveals Differential
916 Transcription Profile Sharpening of Endocytic Proteins in Cochlear Hair Cells Upon
917 Maturation. Front Cell Neurosci [Internet]. 2021 Feb 26;15. Available from:
918 https://www.frontiersin.org/articles/10.3389/fncel.2021.643517/full

919 43. No Title [Internet]. Available from: https://www.biosearchtech.com/support/tools/design-

software/stellaris-probe-designer

44. Schindelin J, Arganda-Carreras I, Frise E, Kaynig V, Longair M, Pietzsch T, et al. Fiji: an open-source platform for biological-image analysis. Nat Methods [Internet]. 2012 Jul 28;9(7):676–82. Available from: http://www.nature.com/articles/nmeth.2019

45. Collman F, Buchanan J, Phend KD, Micheva KD, Weinberg RJ, Smith SJ. Mapping Synapses by Conjugate Light-Electron Array Tomography. J Neurosci [Internet]. 2015 Apr 8;35(14):5792–807. Available from: https://www.jneurosci.org/lookup/doi/10.1523/JNEUROSCI.4274-14.2015

46. A Stable Lead by Modification of Sato's Method. J Electron Microsc (Tokyo) [Internet]. 1986 Oct; Available from: https://academic.oup.com/jmicro/article/35/3/304/847425/A-Stable-Lead-by-Modification-of-Satos-Method

940
941 **FIGURES/LEGENDS**

942 **FIGURE 1**

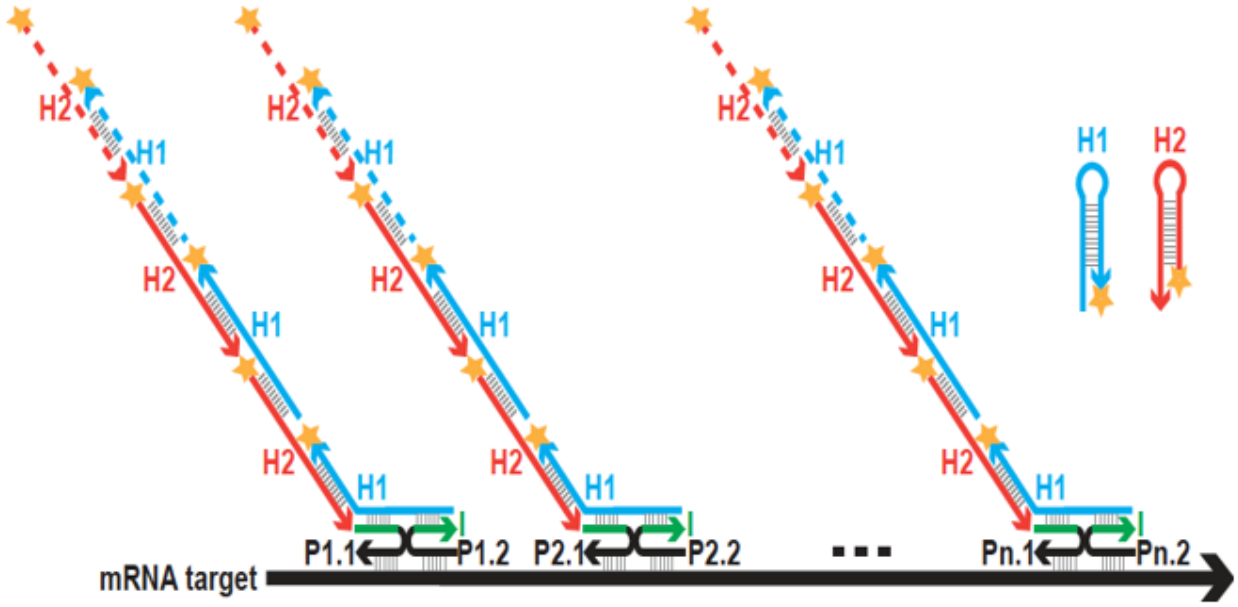

943

944

945

946

947

948

949

950

951

952

953 **Figure 1. HCR Mechanism.** A. The HCR mechanism using split initiator probe pairs. Each anti-
954 sense oligonucleotide probe carries one half of a unique initiator sequence. Once both probes
955 in a pair (P1.1 and P1.2, P2.1 and P2.2, etc.) bind the target mRNA the complete initiator
956 sequence is then available for the fluorescently labeled hairpins (H1 and H2) to self-assemble a
957 tethered polymer. The five unique initiator sequences allow multiple target mRNA's to be probed
958 and amplified simultaneously utilizing hairpins conjugated to spectrally separated fluorophores.

959

960

961

962

963

964

965

966

967

968

969

970

971

972

973 **FIGURE 2**

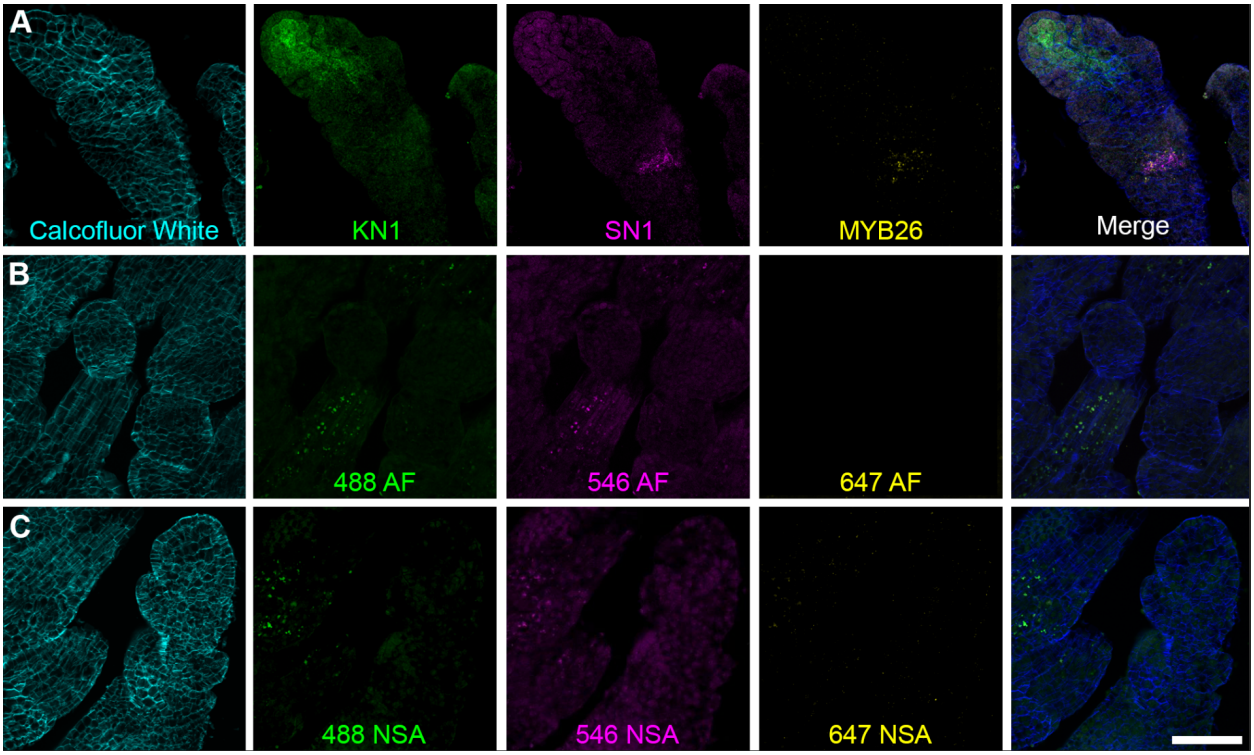

974

975

976

977

978

979

980

981

982

983 **Figure 2. HCR detected multiple mRNA transcripts simultaneously in paraffin sections of**
984 ***Setaria* inflorescences.** A-C. Longitudinal plane through 10 µm paraffin sections of 17-day
985 *Setaria viridis* florets imaged with a 63x/1.2 NA water immersion objective. A single 1.37µm
986 optical slice is shown. A. HCR for KN1, SH1 and MYB26 HCR. KN1: homeotic protein
987 KNOTTED1 (Alexa Fluor 488), SH1: YABBY 2-like protein (Shattering1, Alexa Fluor 546),
988 MYB26: transcription factor MYB86-like (Alexa Fluor 647). B. Autofluorescence (AF) control. No
989 HCR probes or hairpins were used. C. Non-specific amplification control (NSA). Fluorescent
990 hairpins only were used. Cell walls were labeled with Calcofluor White. Scale = 40 µm.

991

992

993

994

995

996

997

998

999

1000

1001

1002

1003 **FIGURE 3**

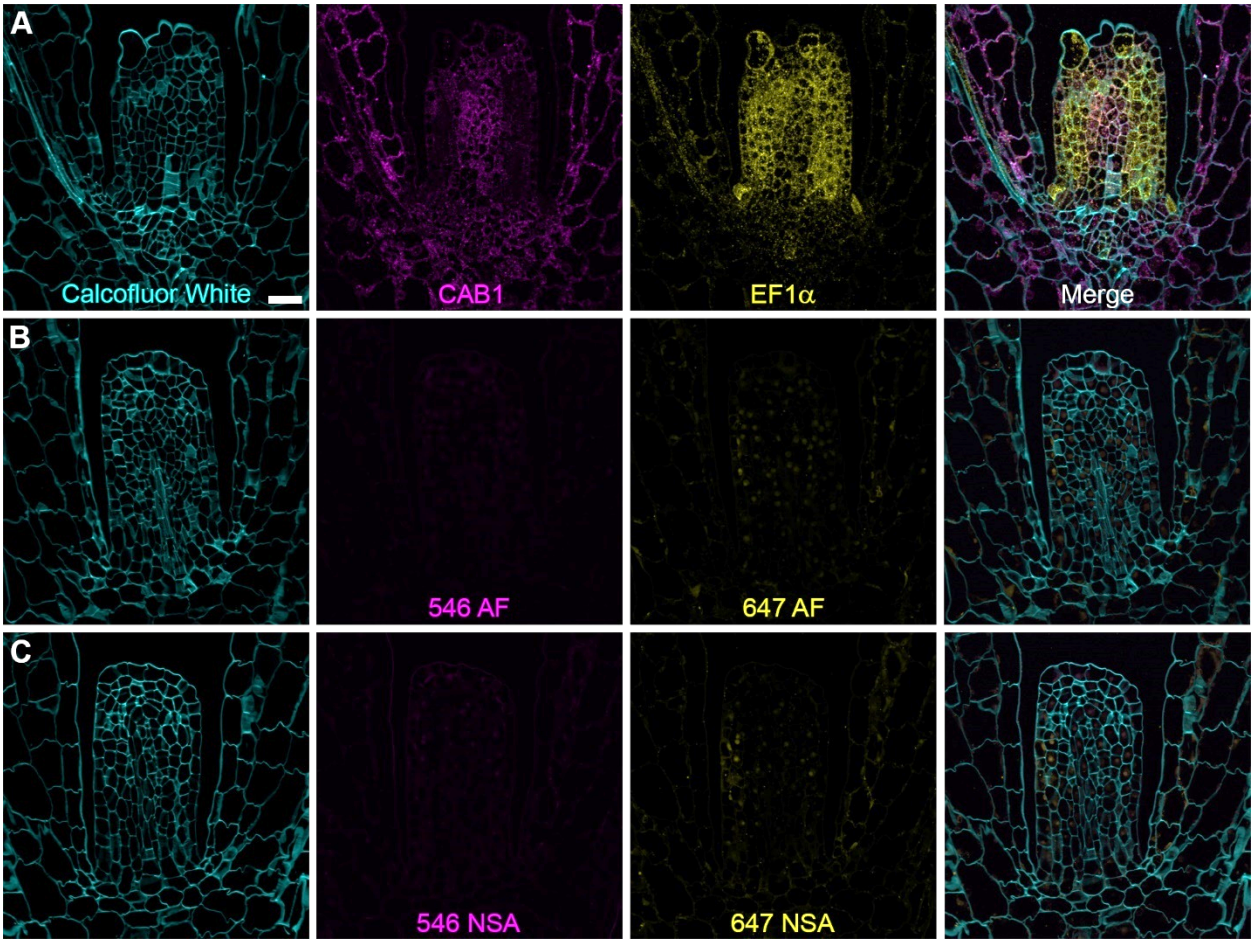

1004

1005

1006

1007

1008

1009

1010

1011 **Figure 3. HCR detected multiple mRNA transcripts simultaneously in methacrylate**
1012 **sections of *Arabidopsis* seedling.** A-C. Longitudinal plane through 1.5μm methacrylate
1013 sections of 3-day *Arabidopsis thaliana* stem apex and cotyledons imaged with a 63x/1.2 NA
1014 water immersion objective. A single 1.37μm optical slice is shown. A. HCR for CAB1
1015 (AlexaFluor 546) and EF1α (AlexaFluor 647). CAB1: chlorophyll binding protein a/b, EF1α:
1016 elongation factor 1 alpha. B. Autofluorescence (AF) control. No HCR probes or hairpins were
1017 used. C. Non-specific amplification control (NSA). Fluorescent hairpins only were used. Cell
1018 walls were labeled with Calcofluor White. Scale = 20μm

1019

1020

1021

1022

1023

1024

1025

1026

1027

1028

1029

1030

1031 **FIGURE 4**

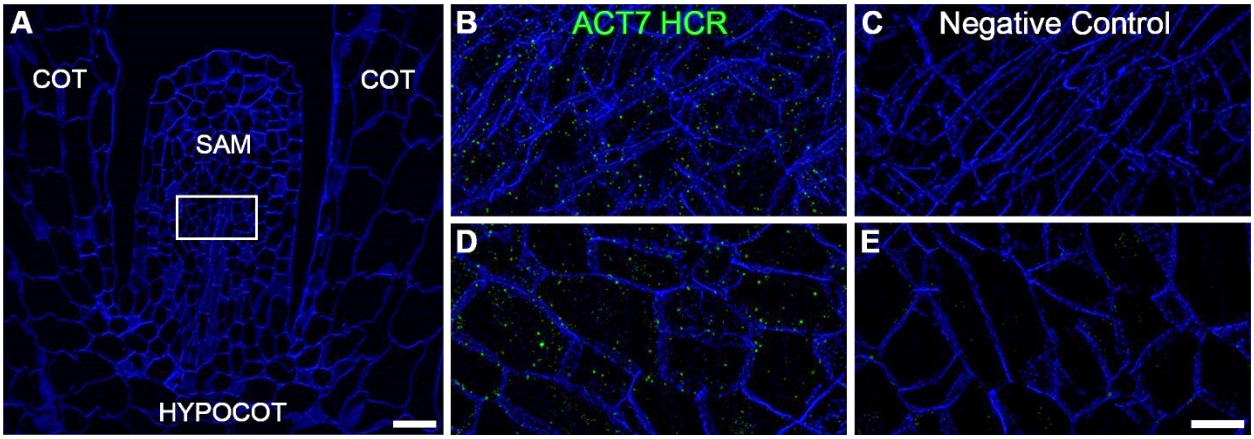

1032

1033

1034

1035

1036

1037

1038

1039

1040

1041

1042

1043

1044

1045 **Figure 4. Lattice SIM imaging improved detection sensitivity of low intensity HCR signal.**
1046 A. A representative confocal microscope image of a 3-day-old *Arabidopsis thaliana* seedling
1047 sectioned longitudinally through the shoot apical meristem (SAM), cotyledons (COT) and
1048 hypocotyl (HYPOCOT). The bounding box indicates the relative location of B-E. Scale = 20 μm.
1049 B. Lattice SIM image of HCR for ACT7 (green) labeled with Alexa Fluor 488 in a 10μm thick
1050 paraffin section. C. Alexa Fluor 488 hairpin only control for non-specific amplification (NSA) in a
1051 10 μm paraffin section. D. HCR for ACT7 (green) labeled with Alexa Fluor 488 in a 1.5 μm
1052 methacrylate section. E. Green autofluorescence control in a 1.5 μm methacrylate section.
1053 Scale = 5 μm. Cell walls stained with Calcofluor White (blue) in all images. HCR and negative
1054 control lattice SIM images were taken with identical microscope parameters and displayed with
1055 equal pixel brightness settings.

1056

1057

1058

1059

1060

1061

1062

1063

1064

1065

1066 **FIGURE 5**

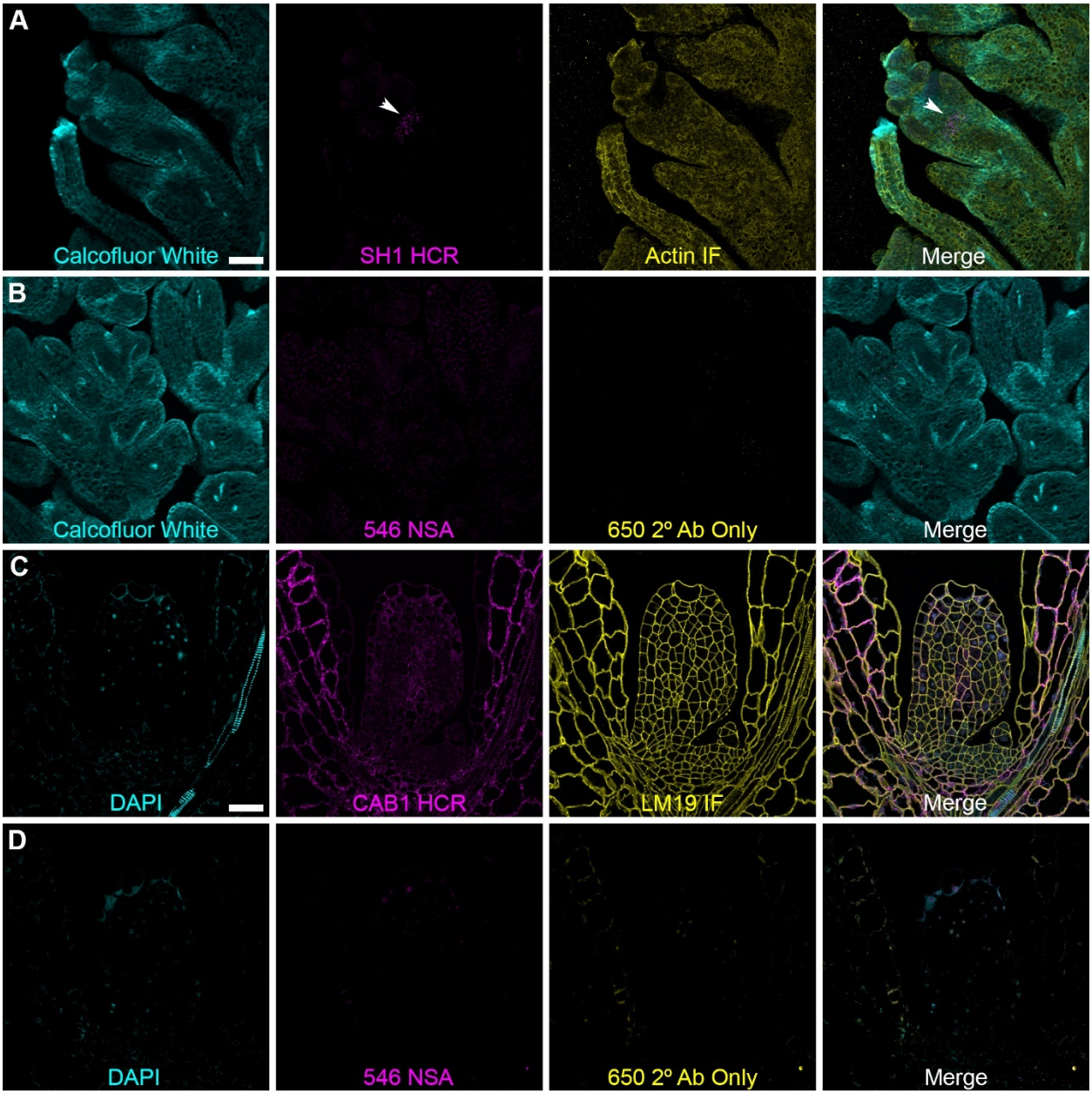

1067

1068

1069

1070

1071 **Figure 5. HCR combined with Immunolabeling in the same sections.** A. 10 µm paraffin
1072 section of the spikelet abscission zone. *SH1*: Shattering 1 mRNA Alexa Fluor 546 (white
1073 arrowhead). Actin immunolabeling: Agrisera AS13 2640 Rabbit anti-actin (100 amino acid
1074 recombinant peptide actin) detected by Agrisera donkey anti-rabbit IgG DyLight 650. 20x 0.7NA
1075 objective, 1.5x zoom, 1.24 AU pinhole = 2.3 µm single optical slice. Scale A & B = 50 µm. B.
1076 Non-specific amplification control using only B2 Alexa Fluor 546 hairpins and donkey anti-rabbit
1077 IgG DyLight 650 secondary antibodies. Brightness set using the HCR & immunolabeling image
1078 then reused on the control images. C. *Arabidopsis* seedling shoot apex in a semi-thin
1079 methacrylate section with LM19 immunolabeling and *CAB1* HCR. 63x objective. Scale C & D =
1080 50 µm D. Non-specific amplification control using only B2 Alexa Fluor 546 hairpins and Donkey
1081 anti-rat IgG DyLight 650 secondary antibodies. Brightness set using the HCR and
1082 immunolabeling image then reused for control images.

1083

1084

1085

1086

1087

1088

1089

1090

1091

1092

1093 **FIGURE 6**

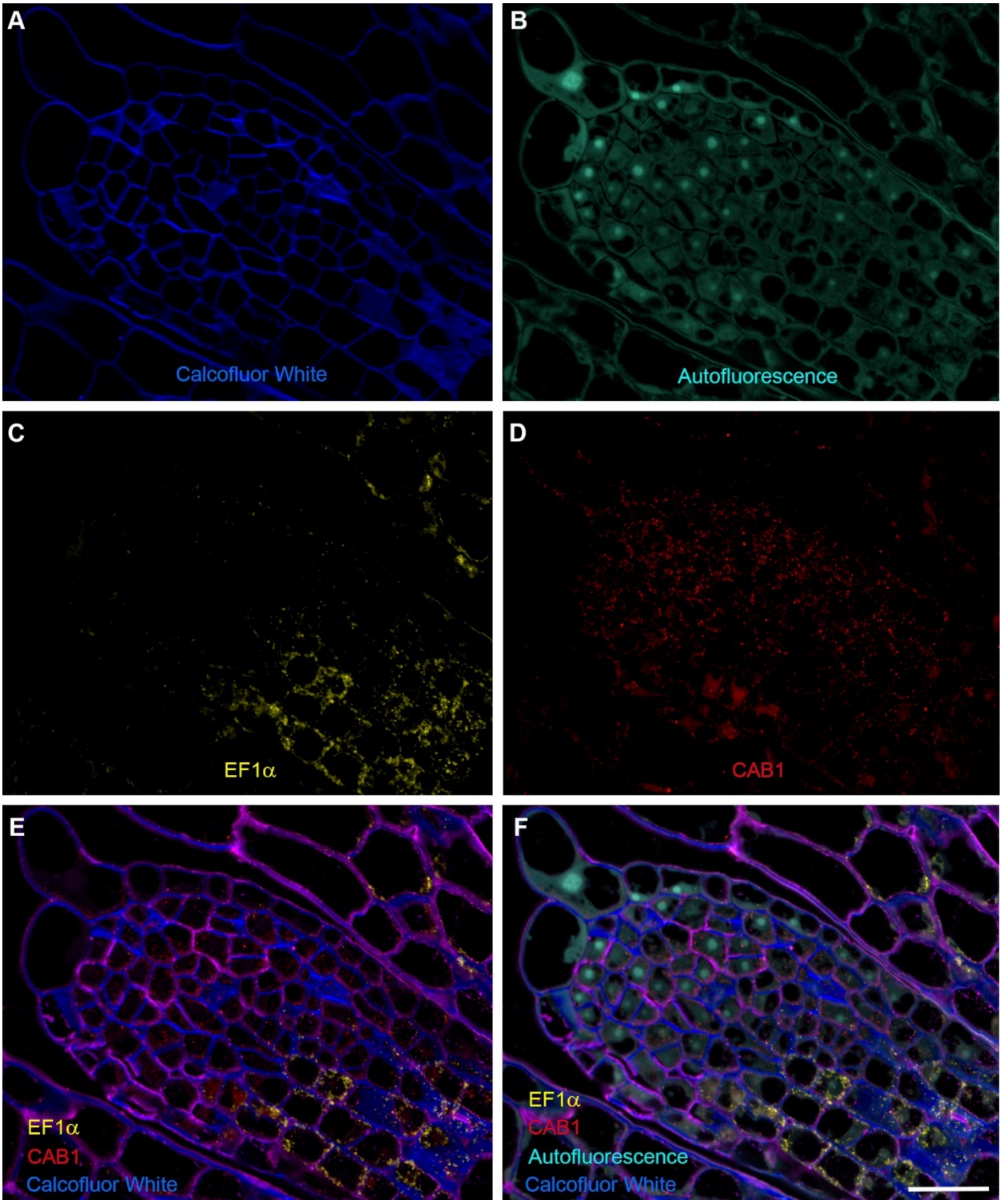

1094

1095

1096 **Fig 6. Spectral linear unmixing of methacrylate de-embedded *A. thaliana* meristem**
1097 **showed improved probe separation from plant autofluorescence.** A 1.5 μm methacrylate
1098 section of an *A. thaliana* meristem labeled with Calcofluor White (A), plant autofluorescence (B),
1099 HCR *EF1α* (C) and HCR CAB1 (D) following linear unmixing using reference spectra for each
1100 dye. The resulting clean signals, following linear unmixing, allowed more definitive separation of
1101 probes, especially from the substantially cytoplasmic autofluorescence (B). Once achieved,
1102 several spectrally distinct fluorescent probes could be combined without (E) or with (F) the
1103 autofluorescence signal. Scale = 20 μm.

1104

1105

1106

1107

1108

1109

1110

1111

1112

1113

1114

1115

1116

1117

FIGURE 7

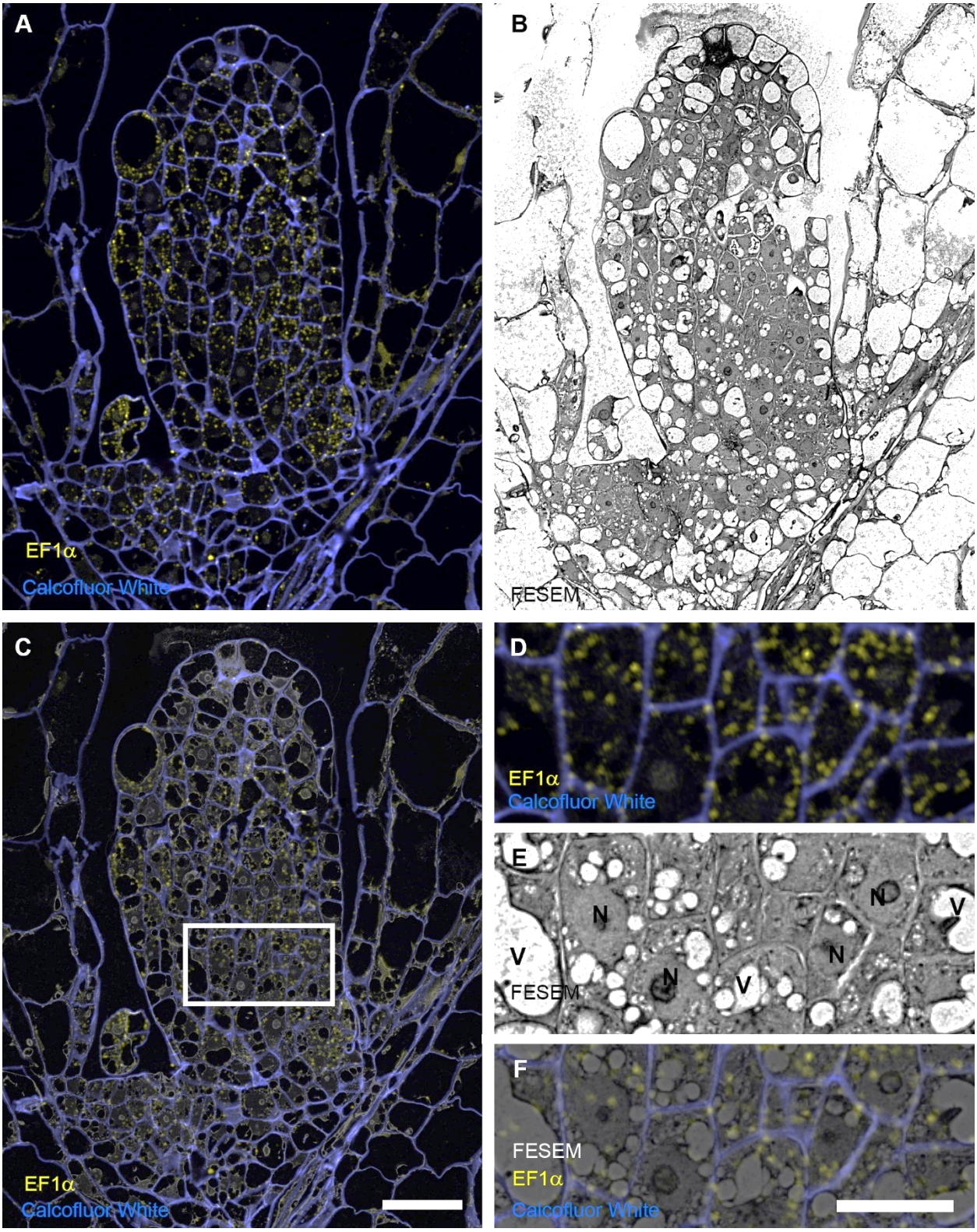

1118

1119 **Figure 7. HCR can be combined with backscatter FESEM with methacrylate de-embedded**
1120 **plant tissues.** (A) Fluorescence image of an *A thaliana* shoot meristem from 0.5 μM section
1121 stained with Calcofluor White (blue) and HCR EF1α (yellow) by confocal microscopy. (B) The
1122 same sample was heavy metal stained and imaged by FESEM using back-scatter electrons at
1123 50nm pixel resolution for correlative microscopy. (C) The FESEM image intensities (from B)
1124 were then grayscale inverted and overlaid with the corresponding fluorescence mage (A) to
1125 yield a correlative light and electron microscopy image. The white box in C was enlarged to
1126 show corresponding fluorescence (D), FESEM (E) and combined correlated dataset (F) Scale in
1127 A to C = 50 μm, D to F = 20 μm.

1128

1129

1130

1131

1132

1133

1134

1135

1136

1137

1138

1139

1140

FIGURE 8

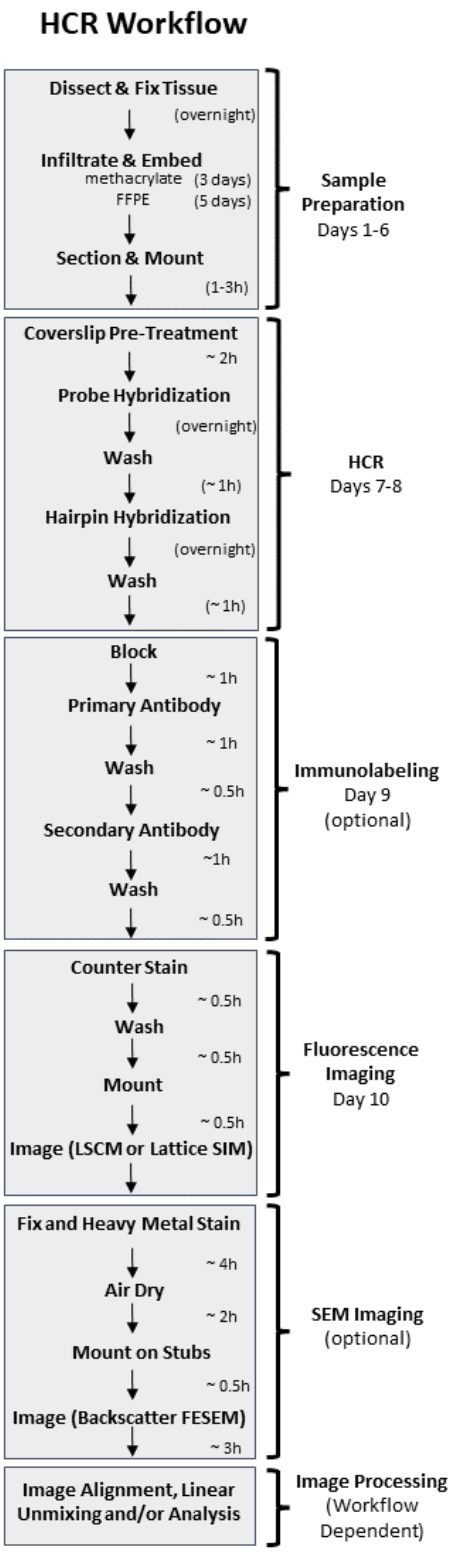

1141

1142 **Figure 8**. **Representative HCR workflow and durations.** The majority of experimental time
1143 involves preparation for sample fixation and generating tissue sections. Immunolabelling
1144 following HCR and/or SEM for correlative ultrastructure is optional. Probe sets that produce
1145 relatively low signals (below the detection limit of laser scanning confocal microscopy (LSCM))
1146 may be imaged with super-resolution lattice structured illumination microscopy (SIM) or other
1147 high quantum efficiency imaging modalities.

1148

1149

1150

1151

1152

1153

1154

1155

1156

1157

1158

1159

1160

1161

1162 **SUPPLEMENTARY FIGURE S1**

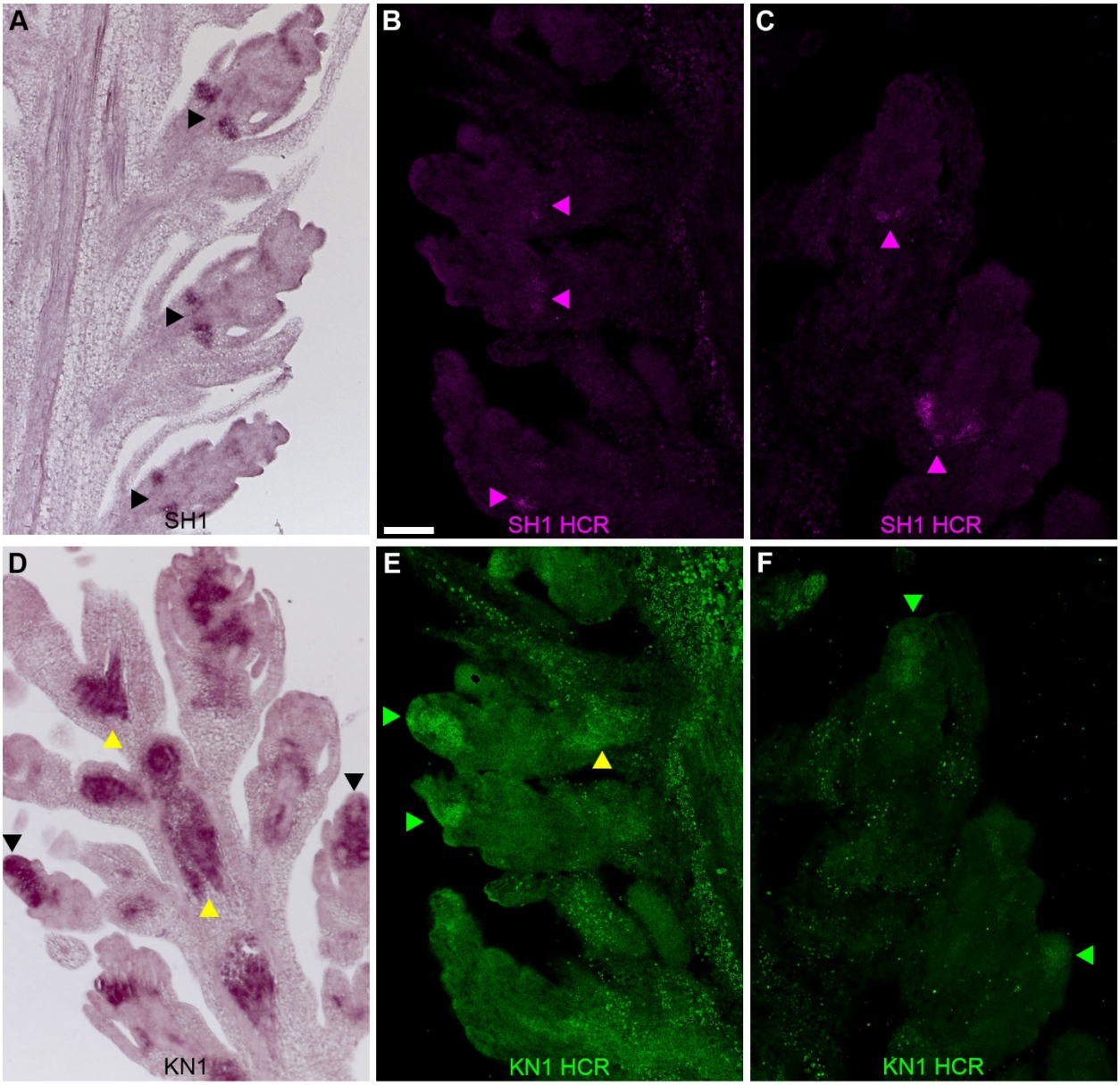

1163

1164

1165

1166

1167

1168 **Figure S1. Localization patterns for SH1 and KN1 in parμμμfin embedded *Setaria viridis***
1169 **spikelets are consistent using both HCR and conventional ISH.** A-F. 10 μm paraffin
1170 longitudinal sections through the panicle of *Setaria viridis*. A. Light micrograph of colorimetric
1171 ISH against Shattering 1 (SH1). Black arrows indicate SH1 expression in the abscission region
1172 of three spikelets. B-C. Confocal images of HCR detection of SH1 using Alexa Fluor 546
1173 conjugated B2 hairpins. Magenta arrows indicate SH1 transcript expression in the abscission
1174 zone of multiple spikelets. D. Light micrograph of colorimetric ISH against the gene *Knotted* 1
1175 (KN1). Black arrows indicate KN1 expression in the meristem region of two spikelets. KN1
1176 expression is also seen in the vascular meristem (yellow arrows). E-F. Confocal microscope
1177 images of HCR detection for KN1 using Alexa Fluor 488 conjugated B4 hairpins. Green arrows
1178 indicate KN1 transcript expression in the rounded meristem tissue of multiple spikelets. Yellow
1179 arrows indicate KN1 expression in the vascular tissue. A pixel intensity threshold was applied to
1180 reduce the saturated non-specific puncta in E-F. Scale = 50 um.
1181
1182
1183
1184
1185
1186
1187
1188
1189

1190 **SUPPLEMENTAL FIGURE S2**

1191

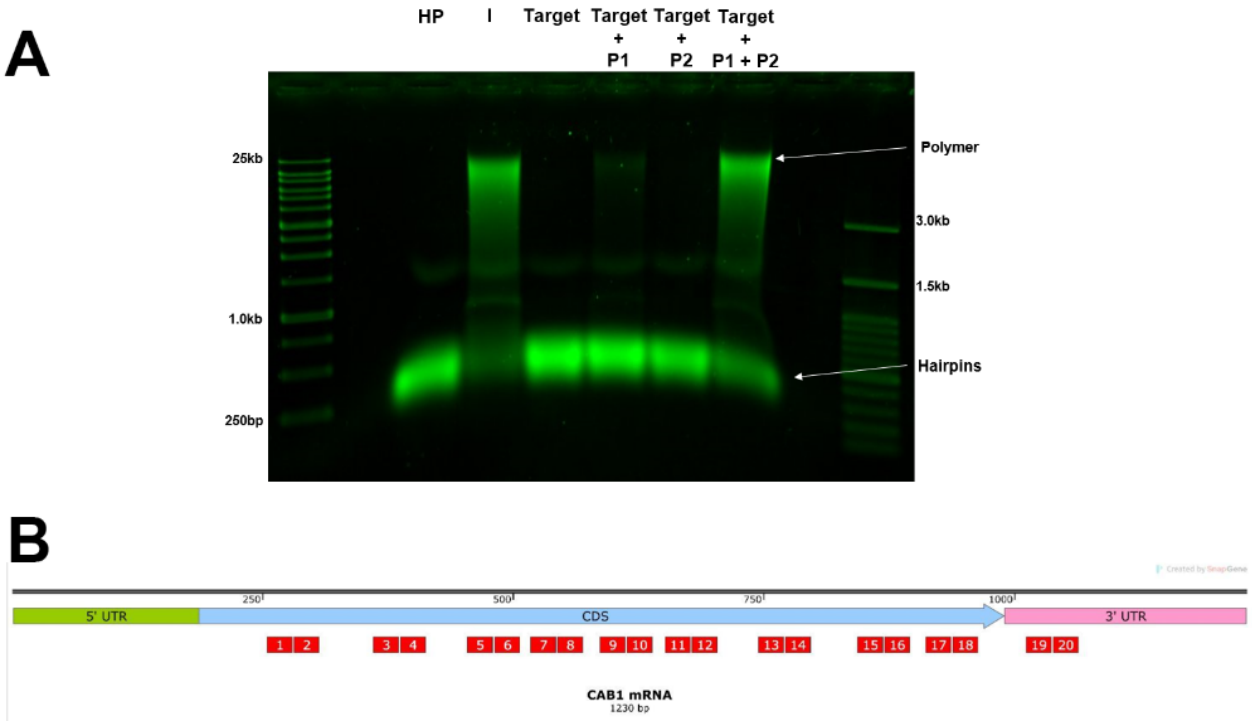

1192

1193

1194

1195

1196

1197

1198

1199

1200

1201 **Figure S2. *In vitro* hairpin assembly**. A. *In vitro* assay confirming the formation of hairpin
1202 polymers only when both split initiator probes in a pair hybridize to the CAB1 target mRNA. HP:
1203 hairpins only. I: B2 initiator sequence. P1: CAB1 probe 1. P2: CAB1 probe 2. 1% agarose/TBE
1204 gel with DNA ladders. B. Map of the mRNA sequence of *Arabidopsis* CAB1. Red boxes indicate
1205 the positions of the HCR probe pairs along the target transcript.

1206

1207

1208

1209

1210

1211

1212

1213

1214

1215

1216

1217

1218

1219

1220

1221 **SUPPLEMENTAL FIGURE S3**

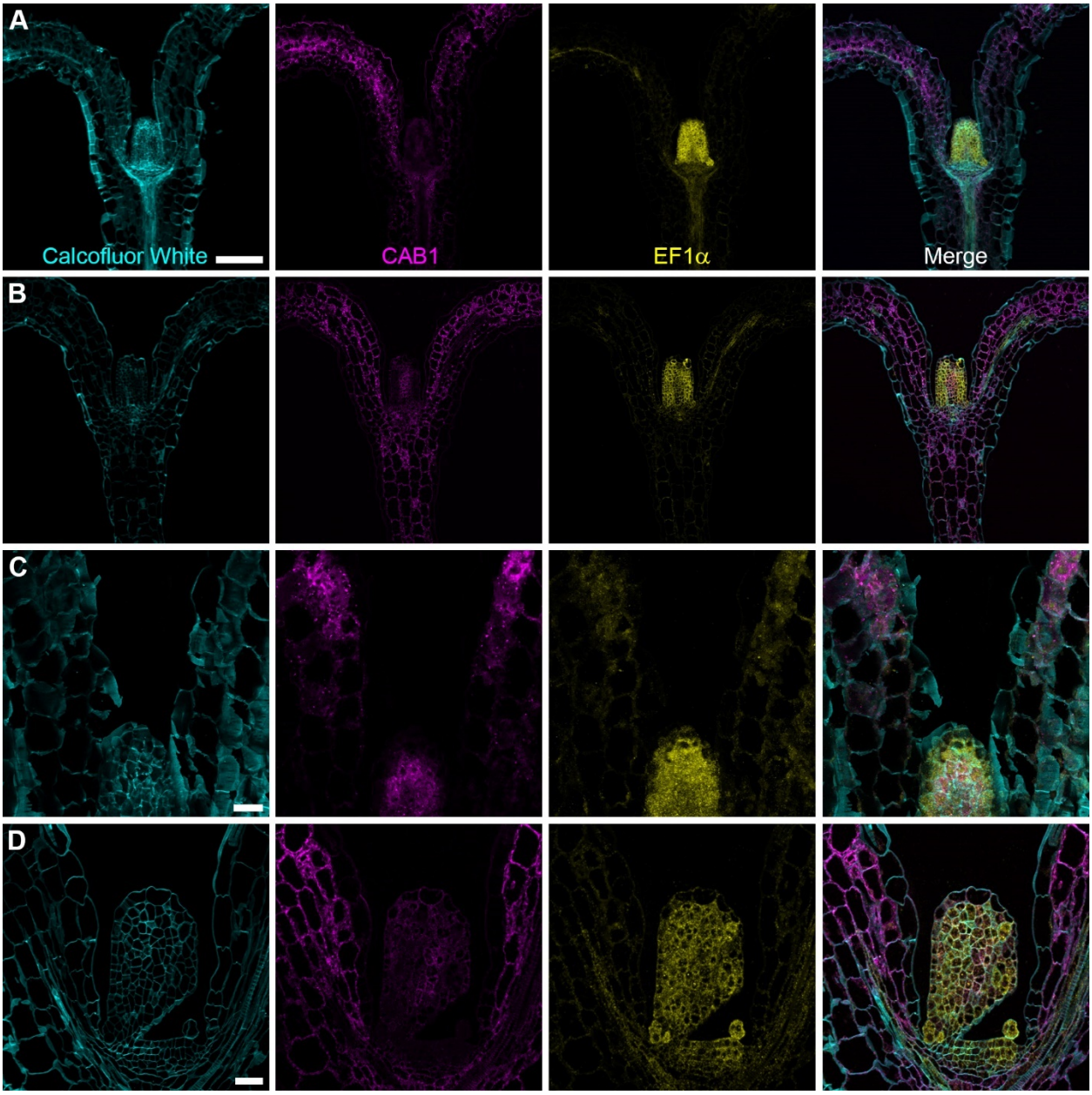

1222

1223

1224

1225

1226

1227 **Fig. S3. Comparison of HCR in paraffin and methacrylate sections.** A-B. 3-day *Arabidopsis*
1228 *thaliana* seedling cotyledons, hypocotyl and shoot apex sectioned in the longitudinal plane and
1229 imaged using a 20x/0.7NA objective. MIP of Z stack. A. 10 µm paraffin section. Scale = 100 µm.
1230 B. 1.5 µm methacrylate section. C-D. 3-day *Arabidopsis thaliana* seedling cotyledons and shoot
1231 apex sectioned in the longitudinal plane and imaged using a 63x/1.2NA water immersion
1232 objective. Single 1.37 µm optical slice. C. 10 µm paraffin section. D. 1.5µm methacrylate
1233 section. Scale = 20 µm. HCR for CAB1 (Alexa Fluor 546) and EF1a (Alexa Fluor 647) with
1234 calcofluor white as a cell wall marker. CAB1: Chlorophyll binding protein a/b. EF1α: Elongation
1235 Factor 1 alpha. Scale = 20 µm.

1236

1237

1238

1239

1240

1241

1242

1243

1244

1245

1246

1247

1248 **SUPPLEMENTAL FIGURE S4**

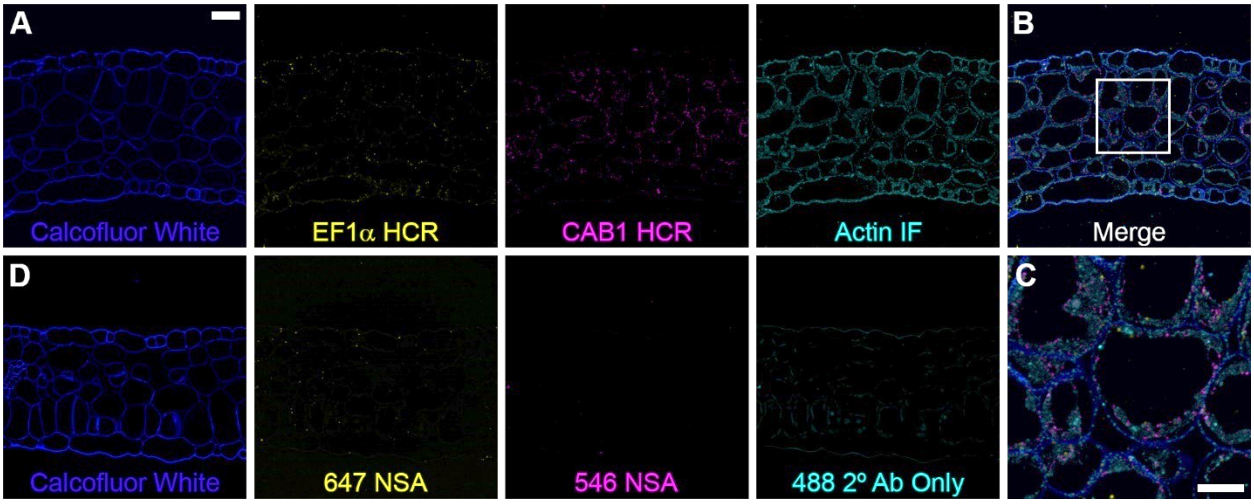

1249

1250

1251

1252

1253

1254

1255

1256

1257

1258

1259

1260

1261

1262 **Figure S4. HCR can be used to detect mRNA transcripts and protein simultaneously in**
1263 **0.5 µm methacrylate sections.** Longitudinal plane through a 3-day *Arabidopsis thaliana*
1264 cotyledon embedded in methacrylate, sectioned at 0.5µm and imaged with a 63x/1.2 NA water
1265 immersion objective. A. Multiplex HCR with IHC. Left to right: Calcofluor White cell wall stain.
1266 HCR for EF1α (Alexa Fluor 647, Elongation factor 1 alpha). HCR for CAB1 (Alexa Fluor 546,
1267 Chlorophyll binding protein a/b). IHC for pan-Actin (DyLight 488). Scale = 20 µm. B. Merged
1268 image. C. Optical zoom of area from bounding box in B. Scale = 10 µm. D. Non-specific
1269 amplification negative control imaged as in A.

1270

1271

1272

1273

1274

1275

1276

1277

1278

1279

1280

1281

1282

1283 **SUPPLEMENTAL FIGURE S5**

1284 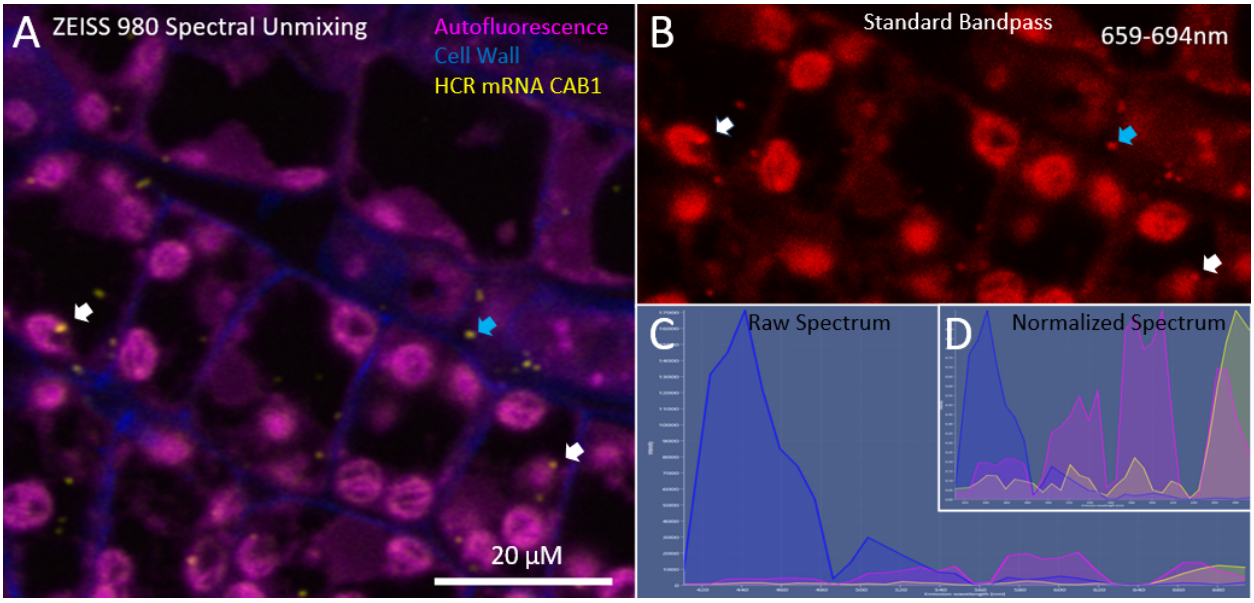

1285

1286

1287

1288

1289

1290

1291

1292

1293

1294

1295 **Figure S5. Linear spectral unmixing and spectra.** A. Linear spectral unmixing of *A. thaliana*
1296 meristem to delineate the cell wall with Calcofluor White (blue), plant autofluorescence
1297 (magenta) and HCR of Alexa Fluor 650 labeled *CAB1* mRNA (yellow). B. Combined signal from
1298 the 659-694 nm (9 nm windows) channels mimicking a standard bandpass filter for Alexa Fluor
1299 650 illustrated the extent of autofluorescence overlap an interference with *CAB1* mRNA probe
1300 (white arrows) while it was possible to distinguish some foci in some areas (blue arrows). This
1301 demonstrated the challenge to clearly localize and/or quantify some signals with highly
1302 autofluorescent tissue or weaker probe signals. (C) Raw and (D) Normalized spectrum of
1303 Calcofluor White (blue), Autofluorescence (magenta) and Alexa Fluor 650 (yellow) spectrum
1304 used for linear unmixing of (A) and showed the extent of autofluorescence overlap and
1305 dominated the green and orange/red emission region of the spectrum. Scale = 20 μm.
1306
1307
1308
1309
1310
1311
1312
1313
1314
1315
1316

1317 **SUPPLEMENTAL FIGURE S6**

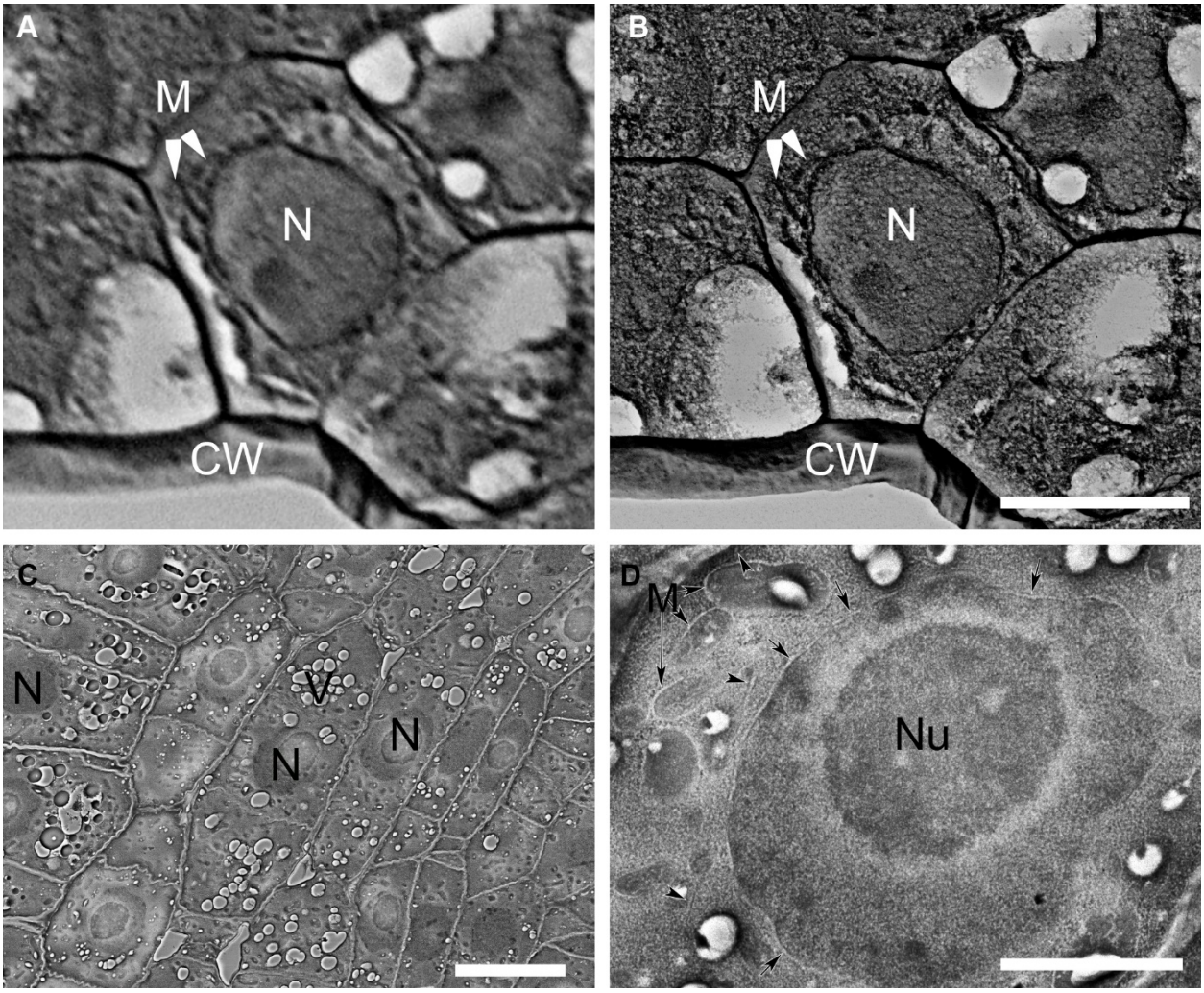

1318

1319

1320

1321

1322

1323

1324

1325 **Figure S6. FESEM of methacrylate de-embedded plant tissues.** A. *A thaliana* shoot
1326 meristem from 1.5 µm section (same specimen/adjacent sections as Fig 6) imaged using back-
1327 scatter electrons at 50nm pixel resolution and B the same location at 5 nm pixel resolution
1328 which showed improved delineation of cell organelles such as the nucleus (N), cell wall (CW)
1329 and mitochondria (M). Scale = 5 µm. C. A portion of an *A. thaliana* root meristem (0.5 µm thick)
1330 in cross-section acquired at 5nm pixel resolution, and at greater magnification (D) showed that
1331 nuclei (N), vacuoles (V), mitochondria (M), the nucleolus (Nu), nuclear envelope (arrows) and
1332 endoplasmic reticulum (arrow heads) are all readily discernable. Scale = 2.5 µm.

1333

1334

1335

1336

1337

1338

1339

1340

1341

1342

1343

1344

1345

SUPPLEMENTAL TABLE 1

Supplemental Table 1

Probe No. *A. thaliana* Chlorophyll Binding Protein A/B (CAB1) HCR System B2

Probe No.	Sequence
1	CCTCGTAAATCCTCATCAAAGCCGCTTCCAAGGACTTCAGATGCC
3	CCTCGTAAATCCTCATCAAAGTGATTCGCCAGAGAATGGACCCAA
5	CCTCGTAAATCCTCATCAAAAGTTCACGGTTCCTTGCGAATGTCT
7	CCTCGTAAATCCTCATCAAAAAAAGCTCAGGGAAGACGCAGCCTA
9	CCTCGTAAATCCTCATCAAACCATCGCTGAAGATCTGTGAACCGG
11	CCTCGTAAATCCTCATCAAATGGCCCAAATGGCCAAAATGCTCTG
13	CCTCGTAAATCCTCATCAAATGCCACCGGGGTAAAGCAAGTCCTC
15	CCTCGTAAATCCTCATCAAACAAACATAGAGAACATAGCCAATCT
17	CCTCGTAAATCCTCATCAAAATCGGCCAAATGGTCAGCAAGGTTC
19	CCTCGTAAATCCTCATCAAAACACTCACGAAGCAAAGACTGAAGC
2	GGCAACAGTCTTCCTCATTGTCACAAAATCATCCAGTAAACCGCC
4	CGGGGAACTCTCCGGTAAGGTAGCTAAATCATCCAGTAAACCGCC
6	ATGGCCCACCTGCTGTGGATAACTTAAATCATCCAGTAAACCGCC
8	TCTCCGAACTTGACTCCGTTTCTAGAAATCATCCAGTAAACCGCC
10	CTAGGGTTTCCCAAGTAATCGAGCCAAATCATCCAGTAAACCGCC
12	CAACGGCTCCCATCAAAATAACTTGAAATCATCCAGTAAACCGCC
14	CGGTAGCCAAACCCAATGGGTCGAAAAATCATCCAGTAAACCGCC
16	CAGTGACGATGGCTTGAACGAAGAAAAATCATCCAGTAAACCGCC
18	GAAGGCCCATGCGTTGTTGTTAACTAAATCATCCAGTAAACCGCC
20	ATCTAAACAAGCTCTCTTTCTCCTCAAATCATCCAGTAAACCGCC

Probe No. *A. thaliana* Elongation Factor 1 alpha (EF1a) HCR System B3

Probe No.	Sequence
1	GTCCCTGCCTCTATATCTTTCAACTTGTAGATCAAGTGTCCAGTG
3	GTCCCTGCCTCTATATCTTTTACTTGAAGGACCTCTTGTTCATCT
5	GTCCCTGCCTCTATATCTTTAGCATCAATGACAGTGCAGTAGTAC
7	GTCCCTGCCTCTATATCTTTTGGAGTCAATGATAAGGACAGCACA
9	GTCCCTGCCTCTATATCTTTGTGAAAGCAAGTAGAGCGTGCTCAC
11	GTCCCTGCCTCTATATCTTTTCCTTGATGATTTCATCGTACCTGG
13	GTCCCTGCCTCTATATCTTTAGAGATGGGCACAAATGGGATTTTG
15	GTCCCTGCCTCTATATCTTTAGGCTTGATCATACCAGTCTCAACA
17	GTCCCTGCCTCTATATCTTTTTGTCACCTGGAAGTGCCTCAAGAA
19	GTCCCTGCCTCTATATCTTTCTGTCAATCTTGGTCAAGATCTCAG
2	CTCAATGACACGCTTGTCAATACCATTCCACTCAACTTTAACCCG
4	GCCTTAAGTTTGTCCAAAACCCATGTTCCACTCAACTTTAACCCG
6	GTTCTTGATGAAATCACGATGGCCATTCCACTCAACTTTAACCCG
8	AGATACCAGCCTCAAAACCACCAGTTTCCACTCAACTTTAACCCG
10	CAGCAGATCATCTGCTTGACACCAATTCCACTCAACTTTAACCCG
12	CCAACCTTCTTCAAGTAGGAAGACATTCCACTCAACTTTAACCCG
14	CTCAATCATGTTGTCACCCTCAAATTTCCACTCAACTTTAACCCG
16	TGTGGGAGCAAAGGTCACAACCATATTCCACTCAACTTTAACCCG
18	GCAACATTCTTAACATTGAACCCAATTCCACTCAACTTTAACCCG
20	TCCTTCTCAATCTCCTTACCAGAACTTCCACTCAACTTTAACCCG

Probe No. *A. thaliana* Actin 7 (ACT7) HCR System B4

Probe No.	Sequence
1	CCTCAACCTACCTCCAACAAATTGGATACTTCAGAGTGAGGATAC
3	CCTCAACCTACCTCCAACAATGAATGGCAACATACATGGCAGGGA
5	CCTCAACCTACCTCCAACAAATCACCAGAATCGAGCACAATACCG
7	CCTCAACCTACCTCCAACAATCTCTCAGTGAGAATCTTCATGAGT
9	CCTCAACCTACCTCCAACAAAAGTTTCTCCTTTATGTCACGGACA
11	CCTCAACCTACCTCCAACAATAGTTCTTCTCCACTGAAGAACTGC
13	CCTCAACCTACCTCCAACAAAGTTGTAAGTTGTTTCATGGATTCC
15	CCTCAACCTACCTCCAACAAACTGAGAACGATGTTTCCATAGAGA
17	CCTCAACCTACCTCCAACAAGATCCAGACACTGTATTTTCTCTCT
19	CCTCAACCTACCTCCAACAATGACTCATCGTACTCACTCTTTGAA
21	CCTCAACCTACCTCCAACAACATCTCAACTAGGGAAAATAGATTT
2	TCCCAGTTACTTACAATACCATGTTATTCTCACCATATTCGCTTC
4	CCACTGGCATAGAGAGAAAGAACGGATTCTCACCATATTCGCTTC
6	GTAGATTGGCACAGTGTGAGACACAATTCTCACCATATTCGCTTC
8	TTCTGCGGTAGTGGTGAACATGTAAATTCTCACCATATTCGCTTC
10	TTGCTCGTAGTCAAGAGCGACATAAATTCTCACCATATTCGCTTC
12	GTTATGACTTGTCCATCAGGTAGCTATTCTCACCATATTCGCTTC
14	TGATATCGACATCACATTTCATGATATTCTCACCATATTCGCTTC
16	AATTCCTGGGAACATGGTGGAACCAATTCTCACCATATTCGCTTC
18	GCTGAGGGATGCAAGGATTGATCCTATTCTCACCATATTCGCTTC
20	GCATTTCCTGTGAACAATCGATGGAATTCTCACCATATTCGCTTC
22	CCACATAACAACAGATAGTTCAATTATTCTCACCATATTCGCTTC

Probe No. *S. viridis* Shattering 1 (SH1) HCR System B2

Probe No.	Sequence
1	CCTCGTAAATCCTCATCAAAACCGCGAGAATTGTGTTGCAGAAGT
3	CCTCGTAAATCCTCATCAAAAAGTGATTGGATCAGTCCTCTCAAG
5	CCTCGTAAATCCTCATCAAAAAAACTGAAATTGTGGACCTTGAGA
7	CCTCGTAAATCCTCATCAAAGTTGGCATCCGGTATTTTGAAGACG
9	CCTCGTAAATCCTCATCAAAATTGTATGCTGAAGGAACACGTTGC
11	CCTCGTAAATCCTCATCAAACTAGGCCAAAATGTATGTTTGGAAA
13	CCTCGTAAATCCTCATCAAAAAGGTTGACAGAAGCAAACACTAAT
15	CCTCGTAAATCCTCATCAAAAGCATTATGTTCTCGTACATATATA
2	TTCAGCATGCTATTACTCGGGACACAAATCATCCAGTAAACCGCC
4	CACCAACTGTGAGTGATTCTGGACAAAATCATCCAGTAAACCGCC
6	TGCATACTCACAGTAGTTTTCAGTAAAATCATCCAGTAAACCGCC
8	TCCTGATCGCCTTTTGTTGAGAACAAAATCATCCAGTAAACCGCC
10	CCTTCGTATCTCTTCCTTAATAAATAAATCATCCAGTAAACCGCC
12	CAAGCTTCTTGCTACTCTCAAGGGGAAATCATCCAGTAAACCGCC
14	ATTTGAATTGGCATGATTGAAGCATAAATCATCCAGTAAACCGCC
16	AACAACATGATGAAGCACTTATTCAAAATCATCCAGTAAACCGCC

Probe No. *S. viridis* MYB86-like transcription factor (MYB26) HCR System B3

Probe No.	Sequence
1	GTCCCTGCCTCTATATCTTTTTGACGAGCTTCTCGTCTTCCTCCG
3	GTCCCTGCCTCTATATCTTTTGGAGTTCCAGAAGTTCTTCACCTC
5	GTCCCTGCCTCTATATCTTTTCCAGAATGTTGTAGTACAGGTCTG
7	GTCCCTGCCTCTATATCTTTTTGATCAATCCATGCATCTATCGAA
9	GTCCCTGCCTCTATATCTTTCCTGAGAAGCTTAACAGTATAATTA
11	GTCCCTGCCTCTATATCTTTAGAAGTTTCAGAGTAGTTCCTCCTT
13	GTCCCTGCCTCTATATCTTTGAATCTCAGCTCATGTTCAGTAACA
2	CAGCCATGGCCGTGAGTGGTGATGTTTCCACTCAACTTTAACCCG
4	CCTGGGAGATGAGCTTCTTCTTGATTTCCACTCAACTTTAACCCG
6	GCGACCGCGATGCCCTGTCCTGCTCTTCCACTCAACTTTAACCCG
8	TAGTATATCTCTGATGCTGCCGCGTTTCCACTCAACTTTAACCCG
10	AACTTATGTGATCACTGGTTTTGCTTTCCACTCAACTTTAACCCG
12	ACACACACTACATATAGCTGTAAATTTCCACTCAACTTTAACCCG
14	AAAAGAGAGGTACAATTTCATGAATTTCCACTCAACTTTAACCCG

Probe No. *S. viridis* Knotted 1 (KN1) HCR System B4

Probe No.	Sequence
1	CCTCAACCTACCTCCAACAAGGAGATGATCTTGGCCTTGATGGCA
3	CCTCAACCTACCTCCAACAAAGAGGAAAGGATATTGCGCAGCGAT
5	CCTCAACCTACCTCCAACAATATACTTCTTCAGGAGATGGTGCTT
7	CCTCAACCTACCTCCAACAATGATCTGCTTCAGGTCAAGCCCAGT
9	CCTCAACCTACCTCCAACAACATATAGAAGGCGCCGGTTGTGTGG
11	CCTCAACCTACCTCCAACAATGGAACCATTAGTGTTTAGCTAGGT
13	CCTCAACCTACCTCCAACAAAACAAAATAATTTAGCATGGCCTCC
15	CCTCAACCTACCTCCAACAAATACAAAAGCAAAAGCACACCACCA
2	GGCGAGGAGCGAGTAGTAGTGAGGGATTCTCACCATATTCGCTTC
4	ACCTTCTTGATCCTCCTCAGAAGAGATTCTCACCATATTCGCTTC
6	CTTGCTTGAGCGAACTCAGATAGCCATTCTCACCATATTCGCTTC
8	GCTTCCGCTGGTTGATGAACCAATTATTCTCACCATATTCGCTTC
10	CCCGCCATCATTGATGAAGTGTCCAATTCTCACCATATTCGCTTC
12	TGGAACCATTAGTGTTTAGCTAGGTATTCTCACCATATTCGCTTC
14	CATAGGCATAGATTGAGTAGCAATGATTCTCACCATATTCGCTTC
16	CATCTGTCAGGTCACACGCATACAAATTCTCACCATATTCGCTTC

1360 **Table S1. Sequences of HCR probes.** All sequences are listed 5' to 3'. The 5' half of the
1361 initiator sequence is shown in magenta while the 3' half of the initiator sequence is shown in
1362 cyan. The spacer sequences are shown in orange. Please refer to the Materials and Methods
1363 section for information on gene accession numbers and probe design.
1364
1365
1366
1367